DMD DRUG METABOLISM AND DISPOSITION aspet

TABLE 1

Literature values of plasma clearance, half-life, unbound fraction in plasma, blood/plasma concentration ratio, and metabolic enzymes in humans for the model compounds examined in this analysis

Rb values of fasudil, lamotrigine, and sulindac were assumed to be 1 due to unavailable data from the literature. References are in Supplemental Tables 1 and 2

Compounds	CL_t or CL_{oral}	$t_{1/2}$	fu	Rb	Metabolic Enzymes
	ml · min^{-1} · *kg*$^{-1}$	*h*			
Dapsone	0.48	22	0.25	1.04	CYP2C9, CYP3A4, NAT
6-Deoxypenciclovir[a,c]	118	–	1	1.2	AO
Diclofenac	3.5	1.4	0.005	0.55	CYP2C9, UGT2B7, UGT1A9
Fasudil	73.2	0.26	0.51	1	AO
Ibuprofen	0.82	1.6	0.006	0.55	CYP2C9, UGT2B7
Ketoprofen	1.6	2.1	0.008	0.55	UGT2B7
Lamotrigine[a]	0.3	–	0.45	1	UGT1A4, UGT2B7
Mirtazapine	8.0	15	0.15	0.67	CYP1A2, CYP2D6, CYP3A4
(*S*)-Naproxen	0.1	–	0.01	0.55	CYP2C9, CYP1A2, UGT2B7
Salbutamol	7.7	3.9	0.925	0.96	SULT1A3
Sulindac[a]	3.3	–	0.060	1	AO
(*S*)-Warfarin	0.055	29	0.015	0.55	CYP2C9
Zaleplon	16	1.1	0.4	0.99	AO, CYP3A4

[a] From oral administration data.
[c] Calculated as famciclovir, which is prodrug of 6-deoxypenciclovir.
–, Unavailable data from intravenous administration.

linearly from 8 to 8.1 min, and the column was re-equilibrated to the initial condition.

Mobile phase condition 2 consisted of 0.1% formic acid (A) and methanol (B) on a YMC-Triart C18 column (3 μm, 50 × 2.1 mm; YMC Co., Ltd., Kyoto, Japan) for the analysis of dapsone, 6-deoxypenciclovir, fasudil, lamotrigine, salbutamol, and zaleplon. The starting condition was 90:10 (A/B). From 0 to 5 min, the mobile phase composition was changed linearly to 10:90 (A/B), and this was maintained until 8 min, then the column was re-equilibrated to the initial condition.

The MS/MS experiments were conducted by using API2000 LC/MS/MS systems (Applied Biosystems, Foster, CA). Mass number of the ionization mode, molecular ion, and product ion for the model compounds were as follows: dapsone *m/z* = 248.99 $[M + H]^+$ to 92.18, 6-deoxypenciclovir *m/z* = 238.05 $[M + H]^+$ to 210.95, diclofenac *m/z* = 294.14 $[M + H]^+$ to 249.53, fasudil *m/z* = 292.07 $[M + H]^+$ to 99.09, ibuprofen *m/z* = 204.88 $[M + H]^+$ to 158.52, ketoprofen *m/z* = 253.16 $[M + H]^+$ to 208.73, lamotrigine *m/z* = 256.03 $[M + H]^+$ to 210.96 mirtazapine *m/z* = 266.14 $[M + H]^+$ to 194.97, (*S*)-naproxen *m/z* = 228.68 $[M + H]^+$ to 168.55, salbutamol *m/z* = 240.18 $[M + H]^+$ to148.03, sulindac *m/z* = 357.07 $[M + H]^+$ to 232.96, (*S*)-warfarin *m/z* = 309.06 $[M + H]^+$ to162.97, zaleplon *m/z* = 306.08 $[M + H]^+$ to 236.12.

Determination of PK Parameters. Pharmacokinetic parameters were determined by noncompartmental methods using the concentration-time curve profile. The total clearances (CL_t) after intravenous administration were calculated as dose/AUC_{∞}. AUC_{∞} values were estimated from the time course using the trapezoidal method with extrapolation from the last quantifiable point to infinity. The terminal elimination $t_{1/2}$ was estimated as $2/ke$, where *ke* is that of the plot of the terminal elimination phase on a logarithmic scale.

Calculation of In Vitro Intrinsic Clearance. In vitro intrinsic clearance ($CL_{int,in\ vitro}$) was calculated from the time course of the disappearance of the test drug during incubation with h-hepatocytes. Each plot was fitted to the first-order elimination rate constant as $C(t) = C_0 * \exp(-ke \cdot t)$, where $C(t)$ and C_0 are the concentration of unchanged test drug at incubation time t and that at preincubation and *ke* is the disappearance rate constant of the unchanged drug.

Subsequently, $CL_{int,in\ vitro}$ (μl · min^{-1} · 10^6 cells^{-1}) values were converted to $CL_{int,in\ vitro}$ (ml · min^{-1} · kg^{-1}) for the whole body. $CL_{int,in\ vitro}$ data were scaled up using physiological parameters, human liver weight 26 g/kg (Davies and Morris, 1993) and PXB mouse liver weight 140 g/kg, and the hepatocellularity (132×10^6 cells/g liver) of PXB mice. These parameters were taken from the average of observed data in PXB mice (RI = 80%).

Calculation of In Vivo Intrinsic Clearance. CL_t of PXB mice was calculated from the plasma concentrations after dosing using noncompartmental methods as described. CL_t was assumed to be equal to the hepatic clearance.

Values of CL_t, plasma unbound fraction (fu), and blood/plasma concentration ratio (Rb) in humans were taken from the literature.

In vivo intrinsic clearance ($CL_{int,in\ vivo}$) was calculated from the in vivo CL_t, fu, Rb, and average hepatic blood flow (Q) based on a well stirred model as $CL_{int,in\ vivo} = CL_t/[(fu/Rb) \times (1 - CL_t/Q)]$ (Pang and Rowland, 1977). These CL_t values were converted to blood clearance using Rb values.

The Q values of humans and PXB mice were set at 21 and 90 ml · min^{-1} · kg^{-1} (same as in normal mice), respectively (Davies and Morris, 1993). In addition, Rb and fu of human were assumed to be equivalent to those of PXB mice. If CL_t of drugs exceeded liver blood flow, then the hepatic clearance was taken as 90% of liver blood flow. $CL_{int,in\ vivo}$ of 6-deoxypenciclovir, lamotrigine, and sulindac were evaluated from oral clearance (CL_{oral}) as $CL_{int,in}/fu/Rb$.

Results

Selection of the Model Compounds for Analysis. In this study, we selected 13 compounds with diverse chemical structures (Fig. 1). Elimination of these selected drugs involves multiple metabolic pathways mediated not only by P450 but also by non-P450 enzymes, such as UGT, SULT, and aldehyde oxidase (AO) in liver. Mirtazapine and warfarin were known to be mainly metabolized by P450. Diclofenac, ibuprofen, and naproxen were metabolized by both UGT and P450. Furthermore, the model compounds metabolized by AO, such as

TABLE 2

Estimation of $CL_{int,in\ vitro}$ (μl · min^{-1} · 10^6 cells^{-1}) in PXB mice hepatocytes and scaling to humans and PXB mice

$CL_{int,in\ vitro}$ (μl · min^{-1} · 10^6 cells^{-1}) values were converted to $CL_{int,in\ vitro}$ (ml · min^{-1} · kg^{-1}) for the whole body. $CL_{int,in\ vitro}$ data were scaled up using physiological parameters, human liver weight (26 g/kg) and PXB mouse liver weight (140 g/kg), and the hepatocellularity (132×10^6 cells/g liver) of PXB mice. Each value represents the mean ± S.D. ($n = 3$).

Compounds	$CL_{int,in\ vitro}$	Scaled $CL_{int,in\ vitro}$ (Human)	Scaled $CL_{int,in\ vitro}$ (PXB Mice)
	μl · min^{-1} · 10^6 cells^{-1}	ml · min^{-1} · kg^{-1}	
Dapsone	2.3 ± 1.2	8.0 ± 4.0	43.1 ± 21.3
6-Deoxypenciclovir	5.3 ± 1.2	18.3 ± 4.2	98.6 ± 22.4
Diclofenac	24.7 ± 1.2	84.7 ± 4.0	455.8 ± 21.3
Fasudil	35.7 ± 13.3	122.4 ± 45.6	659.1 ± 245.4
Ibuprofen	13.3 ± 2.1	45.8 ± 7.1	246.4 ± 38.5
Ketoprofen	6.0 ± 1.0	20.6 ± 3.4	110.9 ± 18.5
Lamotrigine	1.4 ± 1.0	4.8 ± 3.6	25.9 ± 19.2
Mirtazapine	6.3 ± 1.2	21.7 ± 4.0	117.0 ± 21.3
(*S*)-Naproxen	12.7 ± 2.5	43.5 ± 8.6	234.1 ± 46.5
Salbutamol	1.0 ± 1.0	3.3 ± 3.3	17.9 ± 17.8
Sulindac	2.0 ± 2.0	7.0 ± 6.7	37.6 ± 36.0
(*S*)-Warfarin	1.2 ± 0.7	4.1 ± 2.5	22.2 ± 13.3
Zaleplon	2.3 ± 1.2	8.0 ± 4.0	43.1 ± 21.3

DMD DRUG METABOLISM AND DISPOSITION aspet

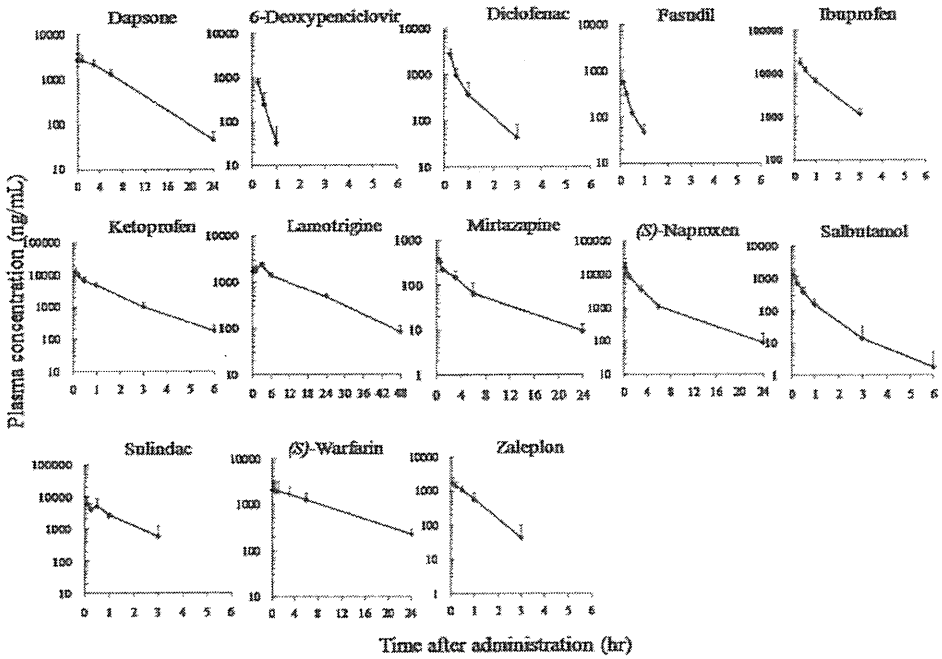

FIG. 2. Plasma concentrations after intravenous administration to PXB mice. Each point represents the mean ± S.D. (n = 3–5).

6-deoxypenciclovir, fasudil, sulindac, and zaleplon, were added in this study. These were reflected in the data set that spanned a wide range of PK parameter characteristics. CL_t and $t_{1/2}$ after intravenous administration of selected model drugs to humans were obtained from the literature. If CL_t after intravenous administration was not available from the literature, we used the value of CL_t/F after oral administration. The PK parameters and the major enzymes responsible for drug metabolism in humans are shown in Table 1. The spreadsheet containing these values with the literature references is included as an attachment in the supplemental data (Supplemental Tables 1 and 2).

Disappearance of Parent Drugs after Incubation. Remaining amounts of all of the compounds decreased linearly to t 2 h on incubation with h-hepatocytes. The values of $CL_{int,in\ vitro}$ in hepatocytes, calculated using scaling factors to humans and PXB mice whole body as described under *Materials and Methods*, are listed in Table 2. These $CL_{int,in\ vitro}$ values covered a wide range. Fasudil showed high clearance, whereas warfarin was very stable.

PK Study of the Model Compounds in PXB Mice. Plasma concentrations and PK parameters in PXB mice after intravenous administration of drug solutions at 0.3 to 5 mg/kg are shown in Fig. 2 and Tables 3 and 4. Each RI value in PXB mice was 73.4 to 93.4%.

CL_t values of warfarin and lamotrigine were relatively low, whereas those of fasudil and salbutamol were much higher; the range of CL_t was 0.2 to 198 ml · min^{-1} · kg^{-1}. The $t_{1/2}$ value of lamotrigine was the longest, and those of 6-deoxypenciclovir and fasudil were short, as shown in Table 3.

Comparison of Intrinsic CL between h-Hepatocytes and Humans. Direct comparison between $CL_{int,in\ vitro}$ from h-hepatocytes and $CL_{int,in\ vivo}$ calculated for a well stirred model in humans showed a moderate correlation (r^2 = 0.475, p = 0.009) (Fig. 3). For 2 of 13 (15%) compounds, observed $CL_{int,in\ vivo}$ was predicted within a 3-fold error from hepatocyte $CL_{int,in\ vitro}$. However, for 8 of 13 (62%) compounds, observed $CL_{int,in\ vivo}$ was predicted with a 3- to 10-fold error.

Figure 4 shows the relationship between $CL_{int,in\ vivo}$ and $CL_{int,in\ vitro}$ for PXB mice; again, the correlation was moderate (r^2 = 0.435, p =

TABLE 3

Experimental conditions and RI values in PXB mice used for PK study

Each compound was administered intravenously to PXB mice at 0.3 to 5 mg/kg body weight. The values of RI of PXB mice ranged from 73.4 to 93.4%. Each value represents the mean ± S.D. (n = 3–5).

Compounds	Dose	RI	CL_t	$t_{1/2}$
	mg/kg	%	ml · min^{-1} · kg^{-1}	h
Dapsone	3.0	77.4 ± 5.5	2.1 ± 0.5	4.5 ± 1.1
6-Deoxypenciclovir	3.0	93.4 ± 4.2	71.2 ± 13.0	0.1 ± 0.1
Diclofenac	3.0	76.4 ± 2.1	16.4 ± 4.3	0.6 ± 0.2
Fasudil	3.0	75.8 ± 1.3	198.1 ± 14.6	0.3 ± 0.1
Ibuprofen	5.0	73.4 ± 3.2	3.8 ± 1.0	0.7 ± 0.1
Ketoprofen	3.0	74.0 ± 1.1	3.3 ± 0.6	1.1 ± 0.1
Lamotrigine	3.0	77.1 ± 4.0	1.4 ± 0.2	10.1 ± 0.9
Mirtazapine	3.0	79.8 ± 1.7	30.4 ± 9.4	6.0 ± 1.4
(*S*)-Naproxen	5.0	82.2 ± 6.1	2.2 ± 0.5	4.8 ± 2.7
Salbutamol	3.0	74.5 ± 0.7	79.9 ± 34.0	0.6 ± 0.3
Sulindac	3.0	74.5 ± 2.0	5.6 ± 1.3	1.2 ± 0.8
(*S*)-Warfarin	0.3	75.3 ± 1.8	0.2 ± 0.1	8.2 ± 2.8
Zaleplon	3.0	77.1 ± 3.7	48.1 ± 7.1	0.7 ± 0.4

TABLE 4

$CL_{int,in\ vivo}$ of humans and PXB mice, calculated by a well stirred model

$CL_{int,in\ vivo}$ was calculated from in vivo CL_t, fu, Rb, and Q based on a well stirred model. The Q values of humans and PXB mice were set at 21 and 90 ml · min^{-1} · kg^{-1} (same as in normal mice), respectively. In addition, Rb and fu of human were assumed to be equivalent to those of PXB mice. If total CL of drugs exceeded liver blood flow, then the hepatic clearance was taken as 90% of liver blood flow. $CL_{int,in\ vivo}$ of 6-deoxypenciclovir, lamotrigine, and sulindac were evaluated from CL_{int} as $CL_{int}/fu/Rb$.

Compounds	Human $CL_{int,in\ vivo}$	PXB Mice $CL_{int,in\ vivo}$
	ml · min^{-1} · kg^{-1}	
Dapsone	2.0	8.6
6-Deoxypenciclovir	118.0	209.0
Diclofenac	1004.3	4905.1
Fasudil	370.6	1588.2
Ibuprofen	147.1	686.0
Ketoprofen	232.2	442.0
Lamotrigine	0.7	3.2
Mirtazapine	125.6	408.7
(*S*)-Naproxen	10.1	230.2
Salbutamol	15.5	1148.2
Sulindac	47.8	86.5
(*S*)-Warfarin	3.7	13.4
Zaleplon	173.6	261.3

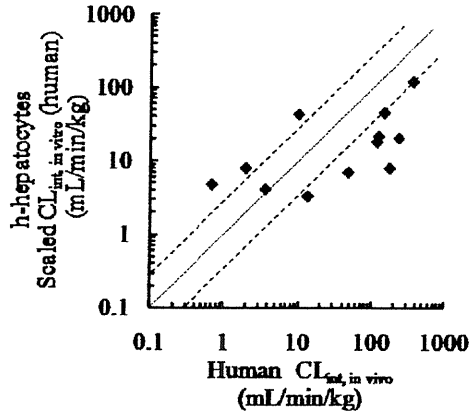

FIG. 3. Correlation between observed human $CL_{int,in\ vivo}$ and $CL_{int,in\ vitro}$ of PXB mouse hepatocytes, calculated as described in the text. The solid line represents unity. The dotted line represents the range within 3-fold of unity.

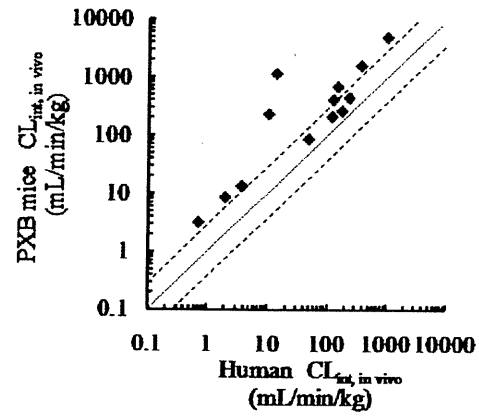

FIG. 5. Correlation of $CL_{int,in\ vivo}$ between humans and PXB mice, calculated as described in the text. The solid line represents unity. The dotted line represents the range within 3-fold of unity.

0.014). For 6 of 13 (46%) compounds, $CL_{int,in\ vivo}$ of PXB mice was predicted within a 3-fold error from h-hepatocyte $CL_{int,in\ vitro}$. For 5 of 13 (38%) compounds, $CL_{int,in\ vivo}$ was predicted within a 3- to 10-fold error.

Relationship between Intrinsic Clearance in Humans and PXB Mice In Vivo. We directly compared $CL_{int,in\ vivo}$ calculated based on a well stirred model in humans and PXB mice. As shown in Fig. 5, there was a good correlation ($r^2 = 0.754$, $p = 1.174 \times 10^{-4}$) between literature $CL_{int,in\ vivo}$ in human and measured $CL_{int,in\ vivo}$ of PXB mice for these compounds. For 4 of 13 (31%) compounds, observed $CL_{int,in\ vivo}$ in humans was predicted within a 3-fold error from PXB mouse $CL_{int,in\ vivo}$. For 7 of 13 (54%) compounds, human $CL_{int,in\ vivo}$ was predicted within a 3- to 10-fold error.

Relationship of Elimination $t_{1/2}$ between Humans and PXB mice. Figure 6 shows the relationship of $t_{1/2}$ after intravenous administration between humans and PXB mice. Compounds for which literature data were not available were excluded from this figure. A good correlation ($r^2 = 0.886$, $p = 1.506 \times 10^{-4}$) was found. For 6 of 9 (67%) compounds, human observed $t_{1/2}$ was predicted within a 3-fold error from PXB mice $t_{1/2}$. For 3 of 9 (33%) compounds, the error was in the range of 3- to 10-fold.

Discussion

The prediction of human PK parameters is an important step during the preclinical development of pharmaceuticals to reduce costs by enabling the early elimination of candidates with unsuitable properties. However, species differences make it difficult to predict human PK from animal data; monkey data may lead to underprediction (Chiou and Buehler, 2002; Akabane et al., 2010), whereas dog data may cause overestimation (Chiou et al., 2000). In vitro-in vivo scaling from data obtained with human hepatic microsomes and hepatocytes is a widely used approach but often results in the underprediction of in vivo CL (Obach, 1999). We considered the possibility that PXB mice, in which hepatocytes are replaced with human hepatocytes to the extent of approximately 80% (Tateno et al., 2004), may have superior predictive utility, because the expression levels and activities of both P450 and non-P450 enzymes well reflect those of the donor hepatocytes (Yoshitsugu et al., 2006; Yamasaki et al., 2010). In this study, we checked metabolic activities (CYP2C9, CYP2D6, UGT, SULT, and AO) using probe substrates between donor hepatocytes and h-hepatocytes purified from PXB mice (Supplemental Table 3) as well as the expression of drug transporters and blood albumin (Tateno et al., 2004; Nishimura et al., 2005).

For the present study, we selected 13 model compounds with diverse chemical structures (Fig. 1), which are metabolized through multiple pathways by P450 and non-P450 enzymes, such as UGT, SULT, and AO. Their values of CL cover a wide range from 0.055 to 118 ml · min^{-1} · kg^{-1} (Table 1).

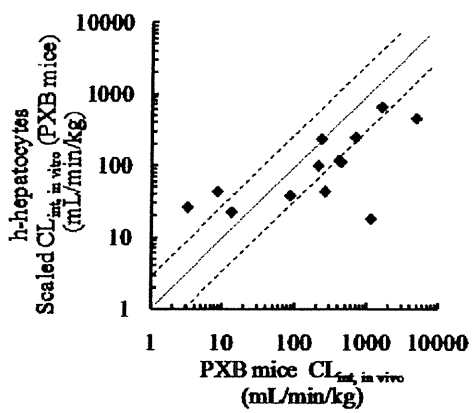

FIG. 4. Correlation between $CL_{int,in\ vivo}$ of PXB mice and $CL_{int,in\ vitro}$ of their hepatocytes, calculated as described in the text. The solid line represents unity. The dotted line represents the range within 3-fold of unity.

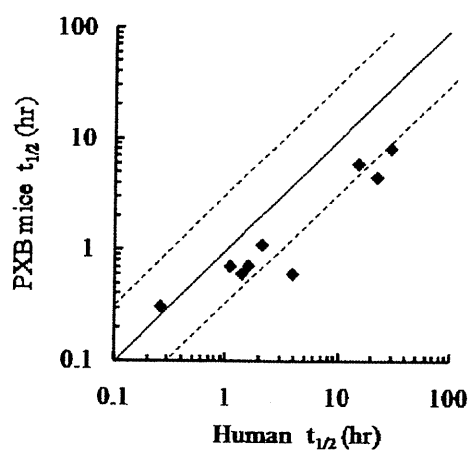

FIG. 6. Correlation of $t_{1/2}$ after intravenous administration between humans and PXB mice. Compounds for which literature data were not available were excluded from this figure. The solid line represents unity. The dotted line represents the range within 3-fold of unity.

First, we performed an in vitro metabolic study using fresh h-hepatocytes isolated from PXB mice. We calculated $CL_{int,in\ vitro}$ using fresh h-hepatocytes and compared the results with human $CL_{int,in\ vivo}$ estimated by use of a well stirred model (Pang and Rowland, 1977). These results using a parallel tube model and a dispersion model were also similar to those of a well stirred model (S. Sanoh, unpublished observations). A moderate correlation ($r^2 = 0.475$, $p = 0.009$) was found, but this approach was not superior to prediction using other methods.

$CL_{int,in\ vitro}$ values of diclofenac, ibuprofen, warfarin, and zaleplon were approximately similar to reported values using cryopreserved hepatocytes (Ekins and Obach, 2000; Nagilla et al., 2006; Stringer et al., 2008), supporting the idea that $CL_{int,in\ vitro}$ values are similar in fresh hepatocytes and cryopreserved hepatocytes (Naritomi et al., 2003; McGinnity et al., 2004).

A similar correlation ($r^2 = 0.435$, $p = 0.014$) was observed between $CL_{int,in\ vitro}$ and $CL_{int,in\ vivo}$ in PXB mice (Fig. 4). In both cases, the numbers of compounds for which absolute values of CL_{int} were predicted within a 3-fold error were insufficient.

Therefore, we next evaluated the predictability of hepatic clearance and $t_{1/2}$ from in vivo data in PXB mice. The values of $CL_{int,in\ vivo}$ estimated by intravenous administration in PXB mice were well correlated ($r^2 = 0.754$, $p = 1.174 \times 10^{-4}$) with observed $CL_{int,in\ vivo}$ in human. Surprisingly, we also found a good correlation ($r^2 = 0.886$, $p = 1.506 \times 10^{-4}$) between $t_{1/2}$ values in PXB mice and humans. However, although the rank order was the same, there were rather large prediction errors, so it may not be possible to predict absolute values. This is consistent with the findings of Xiao et al. (2010) in PXB mice.

We used PXB mice that showed that the average RI values were approximately 80%. It was a concern that the contribution of the remaining approximately 20% mice hepatocytes may be reflected on clearance. $CL_{int,in\ vitro}$ values of these model compounds in host mice hepatocytes (severe combined immunodeficiency mice) were almost higher than those of h-hepatocytes within a 10-fold range (Supplemental Fig. 1). The extent of the difference may not influence the predictability of $CL_{int,in\ vivo}$.

For the estimation of $CL_{int,in\ vivo}$ in PXB mice, the fu values of those model compounds is the same as those in humans because human albumin is expressed in the blood of PXB mice. Inoue et al. (2009) reported fu value of warfarin in PXB mice was similar to that in humans. Furthermore, fu values of some compounds (dapsone, diclofenac, ketoprofen, salbutamol, and zaleplon) in this study were also approximately similar to those in humans (S. Sanoh, unpublished observations).

We assumed that the Rb values of those model compounds is also the same as those in humans, because Rb values of some compounds (dapsone, diclofenac, ketoprofen, salbutamol, and zaleplon) in this study were also approximately similar to those in humans (S. Sanoh, unpublished observations).

Q values were assumed to be 90 ml $\cdot$ min^{-1} $\cdot$ kg^{-1}, respectively, corresponding to the values of normal mice (Davies and Morris, 1993). In further work, it would be desirable to examine whether these values are appropriate.

In this study, we selected model compounds metabolized not only by P450, but also by non-P450 enzymes, including AO. 6-Deoxypenciclovir, fasudil, sulindac, and zaleplon are metabolized mainly by AO in humans. It has been reported that human CL for drugs metabolized by AO may be underpredicted from data obtained with human liver cytosol and S9 due to the loss or deactivation of AO during preparation, homogenization, storage, and experimental procedures (Zientek et al., 2010). PXB mice have high AO activity, being similar to humans (Kitamura et al., 2008), and may be a useful source of fresh h-hepatocytes.

Our results indicate that PXB mice can be used at least for semiquantitative prediction of not only CL_i but also $t_{1/2}$ in humans. PXB mice also would be useful for in vitro estimation and comparison of PK of various candidate compounds, because large amounts of fresh, identical hepatocytes (1.1×10^8 cells/mouse) are available by transplantation of donor hepatocytes (2.5×10^5 cells/mouse). The combination of in vitro study in PXB mice and in vitro study using PXB hepatocytes may prove to be particularly effective.

Acknowledgments

We thank members in PhoenixBio Co., Ltd. for the isolation of hepatocytes from PXB mice.

Authorship Contributions

Participated in research design: Sanoh, Sugihara, Kotake, Tayama, Horie, Kitamura, and Ohta.

Conducted experiments: Sanoh and Horiguchi.

Contributed new reagents or analytic tools: Sugihara, Ohshita, and Tateno.

Performed data analysis: Sanoh and Horiguchi.

Wrote or contributed to the writing of the manuscript: Sanoh, Kotake, Tateno, and Ohta.

References

Akabane T, Tabata K, Kadono K, Sakuda S, Terashita S, and Teramura T (2010) A comparison of pharmacokinetics between humans and monkeys. *Drug Metab Dispos* **38**:308–316.

Brown HS, Griffin M, and Houston JB (2007) Evaluation of cryopreserved human hepatocytes as an alternative in vitro system to microsomes for the prediction of metabolic clearance. *Drug Metab Dispos* **35**:293–301.

Chiba M, Ishii Y, and Sugiyama Y (2009) Prediction of hepatic clearance in human from in vitro data for successful drug development. *AAPS J* **11**:262–276.

Chiou WL and Buehler PW (2002) Comparison of oral absorption and bioavailability of drugs between monkey and human. *Pharm Res* **19**:868–874.

Chiou WL, Jeong HY, Chung SM, and Wu TC (2000) Evaluation of using dog as an animal model to study the fraction of oral dose absorbed of 43 drugs in humans. *Pharm Res* **17**:135–140.

Davies B and Morris T (1993) Physiological parameters in laboratory animals and humans. *Pharm Res* **10**:1093–1095.

De Buck SS, Sinha VK, Fenu LA, Nijsen MJ, Mackie CE, and Gilissen RA (2007) Prediction of human pharmacokinetics using physiologically based modeling: a retrospective analysis of 26 clinically tested drugs. *Drug Metab Dispos* **35**:1766–1780.

De Series M, Bowers G, Boyle G, Beaumont C, Castellino S, Sigaloos J, Dave M, Roberts A, Shah V, Olson K, et al. (2011) Evaluation of a chimeric (uPA+/+/SCID mouse model with a humanized liver for prediction of human metabolism. *Xenobiotica* **41**:464–475.

Ekins S and Obach RS (2000) Three dimensional quantitative structure activity relationship computational approaches for prediction of human in vitro intrinsic clearance. *J Pharmacol Exp Ther* **295**:463–473.

Fagerholm U (2007) Prediction of human pharmacokinetics–evaluation of methods for prediction of hepatic metabolic clearance. *J Pharm Pharmacol* **59**:803–828.

Hallifax D, Foster JA, and Houston JB (2010) Prediction of human metabolic clearance from in vitro systems: retrospective analysis and prospective view. *Pharm Res* **27**:2150–2161.

Huang L, Berry L, Ganga S, Janosky B, Chen A, Roberts J, Colletti AE, and Lin MH (2010) Relationship between passive permeability, efflux, and predictability of clearance from in vitro metabolic intrinsic clearance. *Drug Metab Dispos* **38**:223–231.

Inoue T, Sugihara K, Ohshita H, Horie T, Kitamura S, and Ohta S (2009) Prediction of human disposition toward S-3H-warfarin using chimeric mice with humanized liver. *Drug Metab Pharmacokinet* **24**:153–160.

Kammuri H, Nakada N, Suzuki K, Mera A, Souda K, Murakami Y, Tanaka K, Iwatsubo T, Kawamura A, and Usui T (2010) Assessment of chimeric mice with humanized liver as a tool for predicting circulating human metabolites. *Drug Metab Pharmacokinet* **25**:223–235.

Katoh M, Matsui T, Nakajima M, Tateno C, Kataoka M, Soeno Y, Horie T, Iwasaki K, Yoshizato K, and Yokoi T (2004) Expression of human cytochromes P450 in chimeric mice with humanized liver. *Drug Metab Dispos* **32**:1402–1410.

Katoh M, Matsui T, Okumura H, Nakajima M, Nishimura M, Naito S, Tateno C, Yoshizato K, and Yokoi T (2005) Expression of human phase II enzymes in chimeric mice with humanized liver. *Drug Metab Dispos* **33**:1333–1340.

Kitamura S, Nitta K, Tayama Y, Tanoue C, Sugihara K, Inoue T, Horie T, and Ohta S (2008) Aldehyde oxidase-catalyzed metabolism of N1-methylnicotinamide in vivo and in vitro in chimeric mice with humanized liver. *Drug Metab Dispos* **36**:1202–1205.

McGinnity DF, Soars MG, Urbanowicz RA, and Riley RJ (2004) Evaluation of fresh and cryopreserved hepatocytes as in vitro drug metabolism tools for the prediction of metabolic clearance. *Drug Metab Dispos* **32**:1247–1253.

Nagilla R, Frank KA, Jolivette LJ, and Ward KW (2006) Investigation of the utility of published in vitro intrinsic clearance data for prediction of in vivo clearance. *J Pharmacol Toxicol Methods* **53**:106–116.

Naritomi Y, Terashita S, Kagayama A, and Sugiyama Y (2003) Utility of hepatocytes in predicting drug metabolism: comparison of hepatic intrinsic clearance in rats and humans in vivo and in vitro. *Drug Metab Dispos* **31**:580–588.

Nishimura M, Yoshitsugu H, Yokoi T, Tateno C, Kataoka M, Horie T, Yoshizato K, and Naito

S (2005) Evaluation of mRNA expression of human drug-metabolizing enzymes and transporters in chimeric mouse with humanized liver. *Xenobiotica* **35**:877–890.
Obach RS (1999) Prediction of human clearance of twenty-nine drugs from hepatic microsomal intrinsic clearance data: An examination of in vitro half-life approach and nonspecific binding to microsomes. *Drug Metab Dispos* **27**:1350–1359.
Paixão P, Gouveia LF, and Morais JA (2010) Prediction of the in vitro intrinsic clearance determined in suspensions of human hepatocytes by using artificial neural networks. *Eur J Pharm Sci* **39**:310–321.
Pang KS and Rowland M (1977) Hepatic clearance of drugs. I. Theoretical considerations of a "well-stirred" model and a "parallel tube" model. Influence of hepatic blood flow, plasma and blood cell binding, and the hepatocellular enzymatic activity on hepatic drug clearance. *J Pharmacokinet Biopharm* **5**:625–653.
Stringer R, Nicklin PL, and Houston JB (2008) Reliability of human cryopreserved hepatocytes and liver microsomes as in vitro systems to predict metabolic clearance. *Xenobiotica* **38**:1313–1329.
Tabata K, Hamakawa N, Sanoh S, Terashita S, and Teramura T (2009) Exploratory population pharmacokinetics (e-PPK) analysis for predicting human PK using exploratory ADME data during early drug discovery research. *Eur J Drug Metab Pharmacokinet* **34**:117–128.
Tateno C, Yoshizane Y, Saito N, Kataoka M, Utoh R, Yamasaki C, Tachibana A, Soeno Y, Asahina K, Hino H, et al. (2004) Near completely humanized liver in mice shows human-type metabolic responses to drugs. *Am J Pathol* **165**:901–912.
Wang Q, Jia R, Ye C, Garcia M, Li J, and Hidalgo IJ (2005) Glucuronidation and sulfation of 7-hydroxycoumarin in liver matrices from human, dog, monkey, rat, and mouse. *In Vitro Cell Dev Biol Anim* **41**:97–103.
Xiao G, Bohnert T, Black C, Klunk L, and Gan LS (2010) Evaluation of chimeric mice with humanized liver to predict human intrinsic clearance of drug molecules at preclinical phase. *Drug Metab Rev* **42(S1:)**P60.
Yamasaki C, Kataoka M, Kato Y, Kakuni M, Usuda S, Ohzone Y, Matsuda S, Adachi Y, Ninomiya S, Itamoto T, et al. (2010) In vitro evaluation of cytochrome P450 and glucuronidation activities in hepatocytes isolated from liver-humanized mice. *Drug Metab Pharmacokinet* **25**:539–550.
Yamazaki H, Kanbayashi S, Inoue T, Tateno C, Nishikura Y, Ootsuka K, Harada D, Naito S, Horie T, and Ohta S (2010) Approach for in vivo protein binding of 5-n-butyl-pyrazolo[1,5-a]pyrimidine bioactivated in chimeric mice with humanized liver by two-dimensional electrophoresis with accelerator mass spectrometry. *Chem Res Toxicol* **23**:152–158.
Yoshitsugu H, Nishimura M, Tateno C, Kataoka M, Takahashi E, Soeno Y, Yoshizato K, Yokoi T, and Naito S (2006) Evaluation of human CYP1A2 and CYP3A4 mRNA expression in hepatocytes from chimeric mice with humanized liver. *Drug Metab Pharmacokinet* **21**:465–474.
Zientek M, Jiang Y, Youdim K, and Obach RS (2010) In vitro-in vivo correlation for intrinsic clearance for drugs metabolized by human aldehyde oxidase. *Drug Metab Dispos* **38**:1322–1327.

Address correspondence to: Dr. Seigo Sanoh, Graduate School of Biomedical Sciences, Hiroshima University, Kasumi 1-2-3, Minami-ku, Hiroshima 734-8553 Japan. E-mail: sanoh@hiroshima-u.ac.jp

DMD DRUG METABOLISM AND DISPOSITION aspet

1521-009X/12/4003-474–480$25.00
DRUG METABOLISM AND DISPOSITION
Copyright © 2012 by The American Society for Pharmacology and Experimental Therapeutics
DMD 40:474–480, 2012

Vol. 40, No. 3
42754/3748075

Investigation of Drug-Drug Interactions Caused by Human Pregnane X Receptor-Mediated Induction of CYP3A4 and CYP2C Subfamilies in Chimeric Mice with a Humanized Liver[S]

Maki Hasegawa, Harunobu Tahara, Ryo Inoue, Masakazu Kakuni, Chise Tateno, and Junko Ushiki

Kyowa Hakko Kirin Co., Ltd., Nagaizumi-cho, Sunto-gun, Shizuoka, Japan (M.H., H.T., J.U.); and PhoenixBio, Co., Ltd., Higashihiroshima-shi, Hiroshima, Japan (R.I., M.K., C.T.)

Received September 14, 2011; accepted November 29, 2011

ABSTRACT:

The induction of cytochrome P450 (P450) enzymes is one of the risk factors for drug-drug interactions (DDIs). To date, the human pregnane X receptor (PXR)-mediated CYP3A4 induction has been well studied. In addition to CYP3A4, the expression of CYP2C subfamily is also regulated by PXR, and the DDIs caused by the induction of CYP2C enzymes have been reported to have a major clinical impact. The purpose of the present study was to investigate whether chimeric mice with a humanized liver (PXB mice) can be a suitable animal model for investigating the PXR-mediated induction of CYP2C subfamily, together with CYP3A4. We evaluated the inductive effect of rifampicin (RIF), a typical human PXR ligand, on the plasma exposure to the four P450 substrate drugs (triazolam/CYP3A4, pioglitazone/CYP2C8, (*S*)-warfarin/CYP2C9, and (*S*)-(−)-mephenytoin/CYP2C19) by cassette dosing in PXB mice. The induction of several drug-metabolizing enzymes and transporters in the liver was also examined by measuring the enzyme activity and mRNA expression levels. Significant reductions in the exposure to triazolam, pioglitazone, and (*S*)-(−)-mephenytoin, but not to (*S*)-warfarin, were observed. In contrast to the in vivo results, all the four P450 isoforms, including CYP2C9, were elevated by RIF treatment. The discrepancy in the (*S*)-warfarin results between in vivo and in vitro studies may be attributed to the relatively small contribution of CYP2C9 to (*S*)-warfarin elimination in the PXB mice used in this study. In summary, PXB mice are a useful animal model to examine DDIs caused by PXR-mediated induction of CYP2C and CYP3A4.

Introduction

The induction of cytochrome P450 (P450) enzymes is one of the risk factors for drug-drug interactions (DDIs) (Niemi et al., 2003; Luo et al., 2004). The human pregnane X receptor (PXR) is a key nuclear receptor principally responsible for the induction of several P450 enzymes, including CYP3A4, -2C8, -2C9, -2C19, -2A6, and -2B6 (Niemi et al., 2003; Sinz et al., 2008; Chen and Goldstein, 2009). In addition to P450 enzymes, the expression of several drug transporters, such as multidrug resistance gene (MDR) 1, multidrug resistance-associated protein (MRP) 2, organic anion-transporting polypeptides, and phase II metabolic enzymes, including UDP-glucuronosyltransferase (UGT), sulfotransferase, and glutathione S-transferase, are also regulated by human PXR (Dixit et al., 2007; Nishimura et al., 2008a,b; Sinz et al., 2008).

In humans, CYP3A4 plays a major role in drug metabolism because of its abundant expression in the liver and intestine and its broad substrate specificity. In fact, CYP3A4 contributes to the oxidative metabolism of more than 50% of all currently used drugs (de Wildt et al., 1999; Luo et al., 2004). Therefore, CYP3A4-related DDIs have a major clinical impact. CYP3A4 is the most studied isoform among the P450s in terms of DDIs caused by PXR-related induction of drug-metabolizing enzymes. Both in vitro and in vivo experimental models for CYP3A4 induction have been reported by several pharmaceutical companies (Cui et al., 2008; Kanebratt and Andersson, 2008; Kim et al., 2008, 2010; Kamiguchi et al., 2010).

The human CYP2C subfamily has four members: CYP2C8, CYP2C9, CYP2C18, and CYP2C19 (Lüpple et al., 2003; Chen and Goldstein, 2009). Of these, CYP2C8, CYP2C9, and CYP2C19 are of clinical importance and are collectively responsible for the metabolism of ~20% of clinically used drugs (Chen and Goldstein, 2009). The substrate specificity of CYP3A4 and CYP2C enzymes sometimes overlaps. In that case, the overall contribution of PXR-regulated P450 enzymes in the drug elimination process is relatively large. These observations suggest that new investigations should focus on the DDIs

Article, publication date, and citation information can be found at http://dmd.aspetjournals.org.
http://dx.doi.org/10.1124/dmd.111.042754.
[S] The online version of this article (available at http://dmd.aspetjournals.org) contains supplemental material.

ABBREVIATIONS: P450, cytochrome P450; DDI, drug-drug interaction; PXR, pregnane X receptor; MDR, multidrug resistance gene; MRP, multidrug resistance-associated protein; UGT, UDP-glucuronosyltransferase; RIF, rifampicin; ROS, rosiglitazone; WAR, (*S*)-warfarin; MEP, (*S*)-(−)-mephenytoin; TRZ, triazolam; GAPDH, glyceraldehyde-3-phosphate dehydrogenase; PCR, polymerase chain reaction; G-6-P, D-glucose 6-phosphate; G-6-P-DH, G-6-P dehydrogenase; LC/MS/MS, liquid chromatography-tandem mass spectrometry; AUC, area under the plasma concentration-time curve.

between PXR ligands and CYP2C substrate drugs. The quantitative polymerase chain reaction (PCR) analyses using human hepatocytes have demonstrated that the magnitude of CYP3A4 induction by PXR ligand is the largest followed by CYP2C enzymes, including CYP2C8, CYP2C9, and CYP2C19 (Raucy et al., 2002; Niemi et al., 2003). In fact, DDIs caused by induction of CYP2C enzymes have been also reported (Chen and Goldstein, 2009). However, there has been no systematic in vivo analysis focusing on the differences in the degree of the inductive effects of PXR ligands on the each of these P450 enzymes.

It has been reported that there is a large species difference in ligand recognition by the PXR between rodents and humans (Jones et al., 2000; LeCluyse, 2001). For example, RIF is more selective for human PXR, whereas the synthetic C21 steroid pregnenolone-16[propto]-carbonitrile, is a weak ligand for the human PXR but a potent ligand for rodents (Jones et al., 2000; LeCluyse, 2001). In fact, the expression of mouse Cyp3a is not influenced by the administration of RIF (Ma et al., 2007). The species differences in the ligand recognition of the PXR limit the utility of animal models to predict PXR-related DDIs in humans. In addition, it is known that there are species differences in metabolic patterns, as well as in the contribution of each P450 isoform to drug elimination (Shin et al., 2009; Kamimura et al., 2010). These species differences make it hard to predict human pharmacokinetics from animal data. Recently, several groups, including our own, have generated the humanized mouse models of the PXR and CYP3A4 by gene knockout and transgenic techniques (Xie et al., 2000; Ma et al., 2007; Kim et al., 2008; Scheer et al., 2008; Hasegawa et al., 2011). These models are useful for investigating CYP3A4 induction by human PXR ligands. However, the effect of the human PXR ligand on drug-metabolizing enzymes other than CYP3A4 cannot be examined using these mouse models.

The chimeric mouse with a humanized liver is an alternative mouse model (Strom et al., 2010). This mouse model, designated as the "PXB mouse," has been established by the transplantation of human hepatocytes into urokinase-type plasminogen activator-transgenic severe combined immunodeficient mice (Tateno et al., 2004). The livers of the PXB mice are replaced with more than 70% human hepatocytes, although the remaining 30% are mouse hepatocytes (Strom et al., 2010). It has been reported that the mRNA expression of several P450 enzymes in the PXB mouse liver is induced by RIF treatment and that PXB mice also show similar drug-metabolizing profiles of CYP3A4 and CYP2C substrate drugs to humans (Katoh et al., 2005a,b; Kamimura et al., 2010). The PXB mouse is expected to provide the opportunity to examine the inductive effect of PXR ligands on the plasma profiles of not only CYP3A4 but also CYP2C substrate drugs. This study will provide important information on DDIs caused by CYP2C induction in addition to CYP3A4.

In the present study, we evaluated the inductive effect of three different doses of RIF on the plasma exposure of PXB mice to the substrate drugs of CYP3A4, CYP2C8, CYP2C9, and CYP2C19, which have been reported to have DDIs with RIF in humans. Furthermore, the induction of several drug-metabolizing enzymes and transporters in the liver was also examined by measuring the enzyme activities and mRNA expression levels.

Materials and Methods

Materials. RIF, rosiglitazone (ROS), (*S*)-warfarin (WAR), dextromethorphan hydrobromide monohydrate, and propranolol hydrochloride were purchased from Wako Pure Chemical Industries (Osaka, Japan). Triazolam (TRZ), phenacetin, bupropion, and diclofenac were purchased from Sigma-Aldrich (St. Louis, MO). (*S*)-(−)-Mephenytoin (MEP) was purchased from Toronto Research Chemicals (North York, Canada). $NADP^+$, D-glucose 6-phosphate (G-6-P), and G-6-P dehydrogenase (G-6-P-DH) were purchased from Oriental Yeast (Tokyo, Japan). All other chemicals and solvents were of analytical grade otherwise noted.

Generation of Chimeric Mice with a Humanized Liver. All animal studies were conducted in accordance with the *Guiding Principles for the Care and Use of Laboratory Animals*, and the experimental protocol used in this study was approved by the Committee for Animal Experiments of PhoenixBio Co., Ltd., and Kyowa Hakko Kirin Co., Ltd. The PXB mice were generated as described previously (Tateno et al., 2004). All PXB mice used in the present study were derived from the same donor cryopreserved hepatocytes (BD85, from a 5-year-old black male; BD Biosciences, Franklin Lakes, NJ). The blood concentration of human albumin in the PXB mice was measured according to a previous report (Tateno et al., 2004) to predict the replacement index of human hepatocytes that had repopulated in the host mouse liver. The actual values of the replacement index in PXB mice used in this study ranged from 82 to 94%.

Pharmacokinetic DDI Study in PXB Mice. Male PXB mice (11–12-weeks-old, 18–23 g) were used in this study. The suspensions of RIF prepared with corn oil were given intraperitoneally at doses of 2, 10, and 50 mg/kg to the PXB mice once daily for 4 days. After the 4 days of treatment of RIF, the PXB mice received a mixture of CYP3A4, CYP2C8, CYP2C9, and CYP2C19 substrate drugs orally via cassette dosing. The dosing mixture was prepared by adding a dimethyl sulfoxide solution of each drug to a 0.5% methylcellulose aqueous solution. The dose of each substrate drug was as follows: TRZ (CYP3A4 substrate), 5 mg/kg; ROS (CYP2C8 substrate), 1 mg/kg; WAR (CYP2C9 substrate), 0.1 mg/kg; and MEP (CYP2C19 substrate), 5 mg/kg. Blood samples were collected at 2 h after administration on days 1 and 4 and 0.5, 1, 2, 4, and 7 h on day 5. The blood samples were centrifuged, and the plasma samples obtained were stored at −80°C until the analysis. After blood sampling on day 5, the mice were euthanized, and a piece of the liver was collected and preserved in RNAlater solution (Invitrogen, Carlsbad, CA) to stabilize the RNA. The remaining liver tissue was frozen in liquid nitrogen and stored at −80°C until microsomal preparation.

RNA Isolation and Quantitative Reverse Transcription-PCR. Total RNA was extracted from the liver using an RNeasy Plus mini kit (QIAGEN, Hilden, Germany) and was reverse-transcribed to obtain cDNA using a PrimeScript RT reagent kit (Takara Bio, Shiga, Japan) according to the manufacturer's instructions. SYBR-PCR was performed using an ABI PRISM 7900HT (Invitrogen) with SYBR Premix Ex Taq (Takara Bio). The PCR conditions were as follows: after initial denaturation at 94°C for 5 min, the amplification was performed by denaturation at 94°C for 30 s, annealing at 65°C for 30 s, and extension at 72°C for 30 s for 45 cycles. In all cases, the input cDNA concentrations were normalized to those of glyceraldehyde-3-phosphate dehydrogenase (GAPDH; ΔC_t). The relative mRNA expression was determined by a $2^{-\Delta\Delta C_t}$ calculation. The primer sequences used in the present study are summarized in Table 1. We confirmed that these primers were capable of amplifying human but not mouse genes.

Preparation of Liver Microsomes and Metabolic Assay. Liver microsomes were prepared from the frozen liver tissues as described previously (Sugihara et al., 2001). The reaction conditions for the enzyme activity of each P450 isoform are summarized in Table 2. The optimized substrate concentrations, the microsomal concentrations, and the reaction times were used to determine metabolic activity precisely. A reaction mixture (50 μl) consisted of 100 mM phosphate buffer, pH 7.4, 3 mM magnesium chloride, 8 mM G-6-P, 1 U/ml G-6-P-DH, 0.8 mM $NADP^+$, microsomal protein, and substrate. The reaction was initiated by the addition of an NADPH-generating system (a mixture of magnesium chloride, G-6-P, G-6-P-DH, and $NADP^+$) after preincubation of the mixture without the NADPH-generating system for 5 min at 37°C. The reaction was terminated at the designated time by the addition of ice-cold methanol containing propranolol as an internal standard. The sample was centrifuged, and the supernatant was diluted with water. The metabolite of each substrate was analyzed using a liquid chromatography-tandem mass spectrometry (LC/MS/MS) system.

Pretreatment of Plasma. Two microliters of plasma sample, 2 μl of dimethyl sulfoxide, and 30 μl of the ice-cold methanol containing the internal standard were mixed and centrifuged. The calibration standards were prepared in the same manner as the plasma samples. The supernatant was mixed with 10

TABLE 1

The sequences of the primers for SYBR-PCR

Gene Name	Primer Sequence (5′ 3′)	
	Forward	Reverse
CYP1A2	AGCTTGACCTTCAGCACAGAC	GATAGTGCTCCTGGACTGTTTTC
CYP2B6	CACTCATCAGCTCTGTATTCGG	GTATGGCATTTTGGCTCGG
CYP2C8	CACAGCTAAAGTCCAGCAAGAC	GATGGGCTAGCATTCTTCAGAC
CYP2C9	ACTATCTCATTCCCAAGGGCAC	GTTCACTAGATCTTCAGGGAAGGC
CYP2C19	CAGCTGACTTACTTGGAGCTGG	CCTGCTGAGAAAGGCATGAAG
CYP2D6[a]	GGTGTGACCCATATGACATC	CTCCCCGAGGCATGCACG
CYP3A4	AGTTAATCCACTGTGACTTTGCCC	TCACGATGGAATGCAAGAGG
UGT1A1	TGTTCCCACTTACTGCACAAC	CTTCAAATTCCTGGGATAGTGG
MDR1	GTATTCAACTATCCCACCCGAC	GAGCTGAGTTCCTTTGTCTCCTAC
MRP2	ACATGAGAGTTGGAGTCTACGG	GGATAACTGGCAAACCTGATAC
GAPDH	CCGAGCCACATCGCTCAGAC	ATGACGAACATGGGGGCATCAG

[a] From Katoh et al. (2005a).

mM ammonium acetate, and the mixture was injected into the LC/MS/MS system.

LC/MS/MS Analysis. The concentrations of the substrate drugs (in plasma samples), and metabolites (in microsomal samples) were measured using the LC/MS/MS system consisting of an ACQUITY UPLC (Waters, Inc., Bedford, MA) connected to a 4000 QTRAP mass spectrometer (AB Sciex, Foster City, CA).

For the plasma samples, chromatographic separation was performed on a CAPCELL PAK C18 MGII column (3 μm, 3 mm inner diameter × 35 mm; Shiseido, Tokyo, Japan) using an injection volume of 10 μl (ROS and WAR) or 25 μl (TRZ and MEP) and a run time of 4 min. The elution was conducted at a flow rate of 0.8 ml/min by a linear gradient with the mobile phase, which consisted of 10 mM ammonium acetate in water (A) and methanol (B). The gradient condition of B (%) was as follows: at 0, 0.2, 2.2, 2.21, 3, and 3.01 min, the B% was 80, 80, 25, 10, 10, and 80%, respectively. The mass spectrometry detection was performed by positive ionization electrospray. The multiple reaction monitoring mode was used, and the monitor ions (*m/z* precursor ion > product ion) were as follows: ROS (358.1 > 153.3), WAR (309.6 > 163.5), TRZ (343.4 > 308.1), and MEP (219.6 > 134.4). The plasma concentration ranges of quantification were as follows: ROS (1.07–3570 ng/ml), WAR (0.925–9250 ng/ml), TRZ (0.343–3430 ng/ml), and MEP (2.18–6550 ng/ml).

For the microsomal samples, chromatographic separation was performed on an ACQUITY UPLC BEH C18 column (1.7 μm, 2.1 mm inner diameter × 50 mm; Waters, Milford, MA) using an injection volume of 7.5 μl and a run time of 2.5 min. The elution was conducted at a flow rate of 0.5 ml/min by a linear gradient with the mobile phase, which consisted of 10 mM ammonium acetate in water (A for CYP1A2, CYP2B6, CYP2C9 (7-hydroxywarfarin), CYP2C19, and CYP2D6 assays) or 0.05% formic acid in water (A for CYP2C8, CYP2C9 (4′-hydroxydiclofenac), and CYP3A4 assays) and methanol (B). The gradient condition of B (%) was as follows: at 0, 0.2, 1.5, 2 and 2.01 min, the B% was 95, 95, 5, 5, and 95%, respectively. The mass spectrometry detection was performed by positive ionization electrospray. The multiple reaction monitoring mode was used, and the monitor ions (*m/z* precursor ion > product ion) were as follows: CYP1A2 (acetaminophen, 152.0 > 110.0), CYP2B6 (hydroxybupropion, 256.1 > 238.1), CYP2C8 (*N*-demethyl rosiglitazone, 344.1 > 121.1; 5-hydroxyrosiglitazone, 374.1 > 151.1), CYP2C9 (4′-hydroxydiclofenac, 312.05 > 230.45; 7-hydroxywarfarin, 325.6 > 163.5), CYP2C19 (4′-hydroxymephenytoin, 235.0 > 150.15), CYP2D6 (dextrorphan, 258.1 > 157.1), and CYP3A4 (1′-hydroxytriazolam, 359.1 > 176.1; 4-hydroxytriazolam, 359.1 > 314.1). Although the metabolites concentrations in the microsomal samples were not quantified, we have confirmed the linearity of signal intensities and no signals in the blank samples.

Pharmacokinetic Analysis. The pharmacokinetic parameters for TRZ, ROS, WAR, and MEP were obtained by a noncompartmental analysis. The log-transformed plasma concentrations were plotted against time. The slope of the elimination phase (λ_z) was estimated by linear regression. The maximal plasma concentration (C_{max}) and time to C_{max} (t_{max}) were obtained directly from the observed values. The apparent $t_{1/2}$ was obtained as $\ln 2/\lambda_z$. The area under the plasma concentration-time curve (AUC) from time 0 to the last data point (AUC_{0-t}) was calculated using the linear trapezoidal method. The AUC after the last data point (AUC_{λ_z}) was estimated by extrapolating with λ_z. The sum of AUC_{0-t} and AUC_{λ_z} was regarded as $AUC_{0-\infty}$.

Statistical Analysis. A one-way analysis of variance with a Dunnett's test was performed to assess for significant differences in the pharmacokinetics, metabolic activity in the liver microsomes, and mRNA expression in the liver between vehicle- and RIF-treated groups. The statistical analyses were performed using the SAS software program (SAS Institute, Cary, NC). The criterion for statistical significance was $P < 0.05$.

Results

The Effect of RIF Treatment on the Pharmacokinetics of CYP3A4 and CYP2C Substrate Drugs. The pharmacokinetics of CYP3A4 (TRZ) and CYP2C substrate drugs (ROS, MEP, and WAR) was evaluated after repeated intraperitoneal administration of RIF (2, 10, and 50 mg/kg daily for 4 days) or vehicle to the PXB mice. The plasma concentration-time profiles of the substrate drugs are shown in Fig. 1, and the pharmacokinetic parameters and the AUC decrease (percentage) of substrate drugs are summarized in Table 3. The plasma exposure to TRZ was decreased with increased doses of RIF

TABLE 2

The reaction conditions for P450 enzyme assay using the liver microsomes

P450	Substrate	Metabolite	Substrate Concentration	Microsomal Concentration	Reaction Time
			μM	*mg/ml*	*min*
CYP1A2	Phenacetin	Acetaminophen	5	0.5	20
CYP2B6	Bupropion	Hydroxybupropion	5	0.5	20
CYP2C8	Rosiglitazone	*N*-Demethylrosiglitazone 5-Hydroxyrosiglitazone	2	0.2	20
CYP2C9	(*S*)-Warfarin	7-Hydroxywarfarin	4	1	30
	Diclofenac	4′-Hydroxydiclofenac	4	0.2	30
CYP2C19	(*S*)-(−)-Mephenytoin	4′-Hydroxymephenytoin	20	0.5	20
CYP2D6	Dextromethorphan	Dextorphan	1	0.2	20
CYP3A4	Triazolam	1′-Hydroxytriazolam 4-Hydroxytriazolam	2	0.2	20

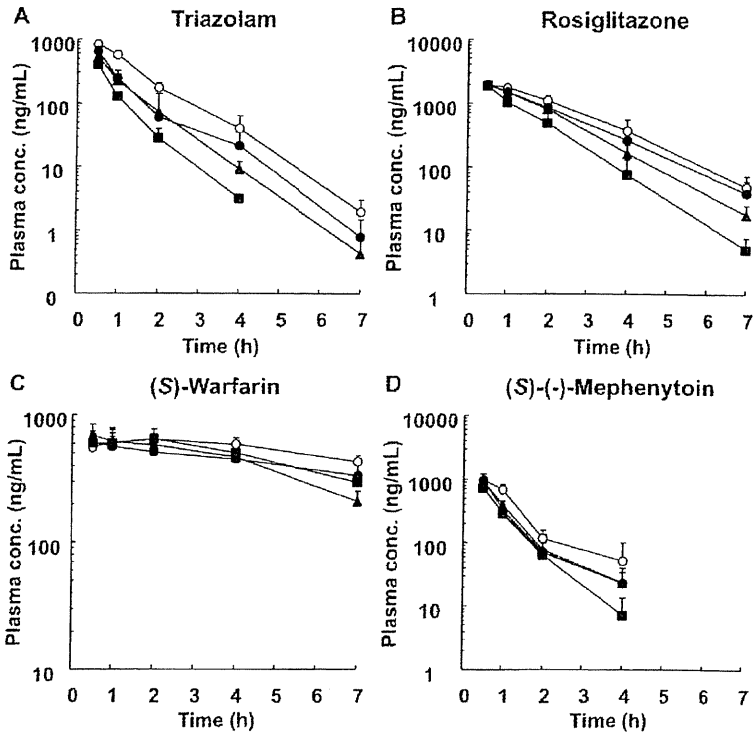

FIG. 1. The plasma concentration-time profiles of TRZ (A), ROS (B), WAR (C), and MEP (D) after repeated intraperitoneal administration of RIF once daily for 4 days to male PXB mice. The PXB mice were given oral doses of 5 mg/kg TRZ (CYP3A4 substrate), 1 mg/kg ROS (CYP2C8 substrate), 0.1 mg/kg WAR (CYP2C9 substrate), and 5 mg/kg MEP (CYP2C19 substrate) via cassette dosing after 4 days of treatment with 2 (●), 10 (▲), or 50 (■) mg/kg RIF or vehicle (○). Each point represents the mean ± S.D. of three mice.

(Fig. 1A). The TRZ AUC was significantly decreased by 46 (2 mg/kg), 54 (10 mg/kg), and 71% (50 mg/kg) compared with the vehicle control (Table 3). RIF treatment also resulted in an AUC decrease of ROS and MEP with increased doses of RIF, and the statistically significance in the AUC decrease was observed only at the dose of 50 mg/kg RIF as 47% for ROS and 46% for MEP (Fig. 1, B and D; Table 3). Treatment with RIF had no effect on the pharmacokinetics of WAR (Fig. 1C; Table 3).

The Metabolic Activities of Human P450 Enzymes in the Liver Microsomes. The metabolic activities of seven human P450 enzymes were determined in the liver microsomes prepared from PXB mice treated with RIF. The fold-induction of enzyme activity for each P450 isoform in the RIF-treated group is shown in Fig. 2. The metabolic activities of CYP3A4 (1′- and 4-hydroxy-TRZ), CYP2C8 (5-hydroxy- and *N*-demethyl-ROS), and CYP2C19 (4-hydroxy-MEP), whose induction was detected in the in vivo study, were significantly increased with increased doses of RIF. Although CYP2C9 induction was not detected in the in vivo study, the metabolic activity of CYP2C9 (7-hydroxy-WAR and 4′-hydroxydiclofenac) was significantly increased by RIF treatment. In addition to CYP3A4 and CYP2C enzymes, the metabolic activities of the CYP1A2, CYP2B6, and CYP2D6 enzymes were also examined. The metabolic activity of CYP2B6 (hydroxybupropion) but not CYP1A2 (acetaminophen) or CYP2D6 (dextrorphan) was increased in a dose-dependent manner by RIF.

TABLE 3

The pharmacokinetic parameters of TRZ, ROS, WAR, and MEP administered orally in cassette dosing after repeated intraperitoneal administration of RIF once daily for 4 days to the male PXB mice

Each value was determined from the data shown in Fig. 1. Data represent the mean ± S.D. of three mice.

		RIF Dose	C_{max}	$t_{1/2}$	$AUC_{0-\infty}$	AUC Decrease
		mg/kg	*ng/ml*	*h*	*ng · h/ml*	*%*
CYP3A4	TRZ	Vehicle	824 ± 92	0.733 ± 0.066	1210 ± 110	
		2	643 ± 72*	0.775 ± 0.055	650 ± 117**	46
		10	408 ± 45**	0.699 ± 0.109	561 ± 205***	54
		50	531 ± 43***	0.575 ± 0.028	346 ± 27***	71
CYP2C8	ROS	Vehicle	1970 ± 240	1.07 ± 0.13	4960 ± 770	
		2	1920 ± 210	1.10 ± 0.18	4120 ± 680	17
		10	1900 ± 350	0.911 ± 0.075	3690 ± 860	26
		50	1850 ± 330	0.772 ± 0.058	2630 ± 900*	47
CYP2C9	WAR	Vehicle	680 ± 26	ND	3830 ± 60	
		2	640 ± 161	ND	3120 ± 830	19
		10	709 ± 197	ND	3420 ± 610	11
		50	715 ± 5	ND	3160 ± 400	18
CYP2C19	MEP	Vehicle	951 ± 250	0.757 ± 0.249	1240 ± 230	
		2	955 ± 150	0.683 ± 0.144	844 ± 173	32
		10	894 ± 102	0.660 ± 0.155	876 ± 84	30
		50	730 ± 61	0.524 ± 0.120	685 ± 198*	46

ND, not determined

Statistically significant from the vehicle-treated group: * $P < 0.05$; ** $P < 0.01$; *** $P < 0.001$.

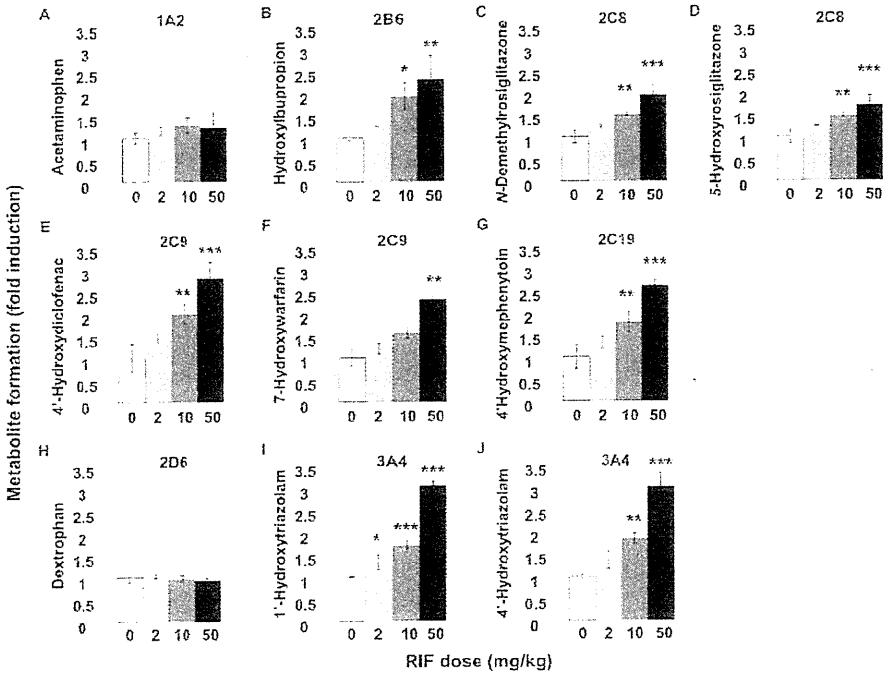

FIG. 2. The metabolic activities of P450 enzymes in the liver microsomes prepared from PXB mice. The liver microsomes were prepared from RIF- or vehicle-treated PXB mice. The activities of P450 enzymes, CYP1A2 (A), CYP2B6 (B), CYP2C8 (C and D), CYP2C9 (E and F), CYP2C19 (G), CYP2D6 (H), and CYP3A4 (I and J), were determined. The experimental conditions are summarized in Table 2. The fold induction in the RIF-treated group compared with vehicle-treated group was calculated. The metabolic activity of each of the mouse liver microsomes was determined from the means of duplicate assay. Each bar represents the mean ± S.D. of three mice. Statistically significant from the vehicle-treated group: *, $P < 0.05$, **, $P < 0.01$, and ***, $P < 0.001$.

The mRNA Expression of Human P450 Enzymes and Transporters. The mRNA expression of the seven human P450 enzymes, UGT1A1, and transporters, including MDR1 and MRP2, was evaluated in the livers of the PXB mice treated with RIF. The fold induction of mRNA expression of enzymes and transporters in the RIF-treated group is shown in Fig. 3. The magnitude of CYP3A4 induction was the largest among the P450 enzymes, followed by CYP2C8 and CYP2B6. Although the enzyme activities of CYP2C9 and CYP2C19 were increased by RIF treatment, the increase in mRNA expression was too slight to detect significant difference. No changes in the mRNA expression of CYP1A2 and CYP2D6 were observed. RIF treatment significantly increased the mRNA expression of UGT1A1, but not MDR1 and MRP2.

Discussion

In the present study, in vivo study using PXB mice, we simultaneously investigated the inductive effect of RIF on CYP3A4 and CYP2C enzymes. We demonstrated that concomitant use of RIF

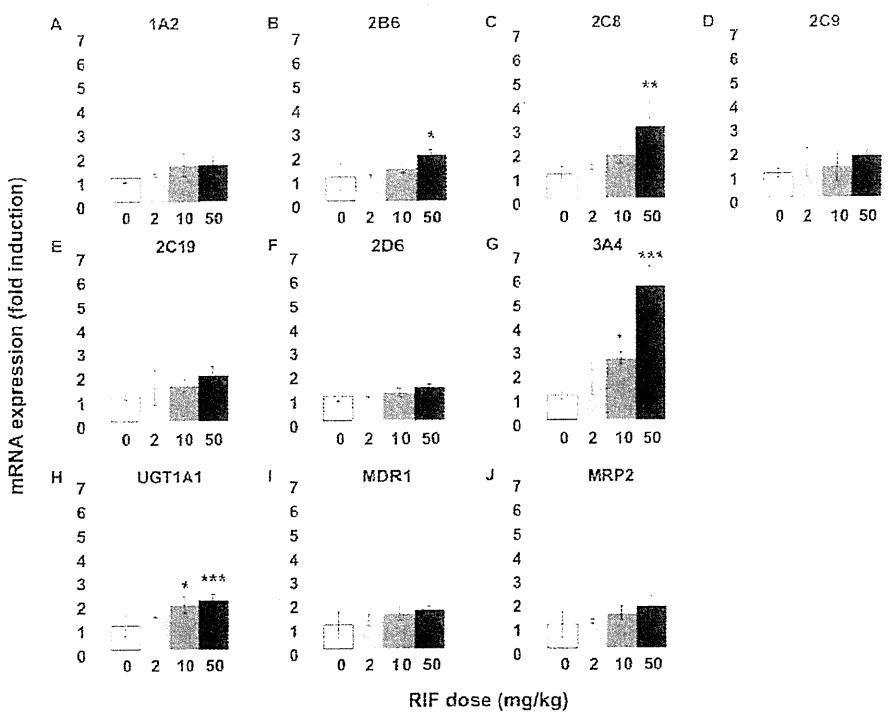

FIG. 3. The mRNA expression levels of P450 enzymes and drug transporters in the liver of PXB mice. The mRNA expression levels of CYP1A2 (A), CYP2B6 (B), CYP2C8 (C), CYP2C9 (D), CYP2C19 (E), CYP2D6 (F), CYP3A4 (G), UGT1A1 (H), MDR1 (I), and MRP2 (J) were determined by SYBR-PCR. The mRNA expression level of each gene was normalized to that of GAPDH. The fold induction in the RIF-treated group compared with vehicle-treated group was calculated. Each bar represents the mean ± S.D. of three mice. Statistically significant from the vehicle-treated group: *, $P < 0.05$, **, $P < 0.01$, and ***, $P < 0.001$.

affects the pharmacokinetics of both CYP3A4 and CYP2C substrate drugs and that the inductive effect of RIF on CYP3A4 is greater than that on CYP2C enzymes. In addition, in vitro studies using the liver samples after RIF treatment were also carried out to examine the enzyme activities of human P450s and the mRNA expression levels of human P450s, UGT, and transporters. The induction by RIF was observed in the genes whose expression levels were known to be regulated by the human PXR, but no change was observed in the genes not regulated by the PXR (CYP2D6).

To compare the pharmacokinetic data between studies conducted in humans and this study, we selected substrate drugs that have previously been reported to have DDIs with RIF in humans. In a clinical study, the AUC decreases in the P450 substrate drug with concomitant use of RIF (600 mg daily) were 46 to 78% (ROS), 57 to 85% (WAR), and 95% (TRZ) (Villikka et al., 1997; Niemi et al., 2003, 2004; Park et al., 2004). The DDI information on CYP2C19 substrate drugs is very limited, and we could only find information about the urinary excretion data for 4′-hydroxymephenytoin, the main metabolite of MEP (Zhou et al., 1990; Feng et al., 1998). The concomitant use of RIF (600 mg daily) increased the urinary excretion of 4′-hydroxymephenytoin from 1.4- to 2.8-fold (Zhou et al., 1990). Assuming that the urinary excretion amount of the metabolite reflects the metabolic clearance of MEP, the decrease in the AUC would be between 29 to 64% as a result of RIF treatment. These reported clinical data suggest that CYP3A4 is the most susceptible to induction by RIF treatment and that the magnitude of induction of CYP2C8, CYP2C9, and CYP2C19 by RIF seems to be relatively weak compared with CYP3A4. In this study using PXB mice, RIF treatment resulted in the largest AUC decrease in TRZ, followed by ROS and MEP (Fig. 1; Table 3). The response to RIF treatment observed in the PXB mice is therefore similar to that in humans.

It was unexpected that the exposure to WAR was not affected by RIF treatment, despite CYP2C9 induction in the liver microsomes (Figs. 1C and 2, E and F; Table 3). The elimination pathways of WAR other than metabolism by CYP2C9 might have made it harder to detect CYP2C9 induction in the in vivo study. In humans, WAR is mainly metabolized to the 7-hydroxyl metabolite by CYP2C9, although WAR is also metabolized to other hydroxyl metabolites by other P450 isoforms (Inoue et al., 2009). Given that the PXB mice used in the present study were derived from the hepatocytes of a single donor, the contribution of CYP2C9 to WAR metabolism in these PXB mice might not be uniformly typical of humans in general. The availability of murine P450 isoforms remaining in the liver of PXB mice could also potentially have affected the overall metabolism of WAR in the in vivo study.

We measured the metabolic activities of WAR in the liver microsomes of SCID (severe combined immunodeficiency) mice (the background strain of the PXB mice) and in pooled human liver microsomes to compare them with PXB mice (supplemental figure). The three types of hydroxyl metabolites of WAR, including 7-hydroxy-WAR, were detected in all of the microsomes. However, the 7-hydroxylation activity in the liver microsomes of PXB mice was only one fifth of that in the human liver microsomes. Therefore, the contribution of CYP2C9 to WAR metabolism in the PXB mice may have been smaller than expected. In fact, the formation of another hydroxyl WAR (M2) in the liver microsomes of SCID mice was greater than that in the human liver microsomes, although the absolute metabolic clearance was not determined (supplemental figure). The metabolic activity of murine P450s remaining in the liver could possibly make it difficult to examine CYP2C9 induction by examining the pharmacokinetics of WAR.

To investigate whether a genetic polymorphism could explain the lower CYP2C9 activity in PXB mice, the CYP2C9 genomic polymorphism was determined by Invader assay (BML, Inc., Tokyo, Tokyo) for the cryopreserved human hepatocytes (lot BD85) used in this study. Although no variant sequence was detected in the CYP2C9 gene (data not shown), real-time quantitative reverse transcription-PCR analysis revealed that the mRNA expression level of CYP2C9 in the hepatocytes was relatively low compared with that in other donor hepatocytes (data not shown). In fact, the plasma elimination of WAR in this study seems to be slower than that in the previous study using PXB mice transplanted with a different lot of human hepatocytes (Inoue et al., 2008). Therefore, the main reason for the failure to detect of CYP2C9 induction in the in vivo study was probably the low hepatic expression of CYP2C9 in the PXB mice used in this study.

In humans, a therapeutic dose of RIF (600 mg) resulted in an $AUC_{0-\infty}$ of 22,400 to 35,300 ng · h/ml (Polk et al., 2001), which was a similar range of plasma exposure as the PXB mouse receiving the 10 mg/kg RIF (M. Kakuni, unpublished data). Considering the AUC decrease of the substrate drugs in PXB mice and humans caused by RIF treatment, the inductive response in PXB mice seems to be relatively weaker than that in humans. It has been reported that CYP3A4, CYP2C8, CYP2C9, and CYP2C19 are expressed in the human intestine (Kolars et al., 1992; Läpple et al., 2003; van de Kerkhof et al., 2008). In addition, it is well known that drug metabolism by intestinal CYP3A4 affects the pharmacokinetics of orally administered drugs (Kato et al., 2003). RIF was previously reported to induce CYP3A4 not only in the liver but also in the intestine in humans (Kolars et al., 1992; van de Kerkhof et al., 2008). Therefore, the decrease in the AUC by concomitant use of RIF in the clinic is accounted for by induction of P450 enzymes both in the liver and in the intestine. In PXB mice, only the liver, but not the intestine, is humanized. Therefore, the intestinal P450 enzymes in PXB mice cannot be induced by RIF, which is a specific human PXR ligand. As a result of the lack of induction in the intestinal P450 enzymes in PXB mice, the reduction of the AUC in the PXB mice would be predicted to be smaller than that in humans. In addition, the hepatic exposure of PXB mice to RIF might be smaller than the expected level, because RIF was administered intraperitoneally, not orally, to PXB mice in this study. The relatively low exposure of the liver to RIF may have result in a weaker induction in the PXB mice.

The induction of CYP3A4 and CYP2C8, CYP2C9, and CYP2C19 by RIF in PXB mice was also demonstrated by examining the enzyme activities using typical substrates for each P450 isoform (Fig. 2). The induction of CYP2B6 in the liver microsomes was also detected (Fig. 2B). This result is consistent with the fact that the expression of CYP2B6 is regulated by the human PXR (Sinz et al., 2008). Next, we determined the mRNA expression levels of other genes, including UGT1A1, MDR1, and MRP2, whose expression levels are also under the regulation of the human PXR (Fig. 3) (Nakata et al., 2006). It was previously demonstrated that RIF led to a small increase in the mRNA expression of these genes using human hepatocytes (Nishimura et al., 2008a,b). In this study, the mRNA expression levels seemed to be slightly increased by RIF in a dose-dependent manner. Statistically significant increase was observed in the mRNA expression levels of UGT1A1 but not in those of MDR1 or MRP2 expression (Fig. 3, H–J). These results might be also attributed to the use of single donor hepatocytes as discussed above.

In the present study, we have performed a DDI study focusing on the human PXR-related induction of CYP3A4 and CYP2C enzymes simultaneously by using the cassette dosing of substrate drugs in PXB mice. We have demonstrated that the PXB mice show a similar response to humans in terms of human PXR-related P450 induction by

RIF. Because the PXB mice used in the present study were derived from the hepatocytes of a single donor, further studies are needed to generalize the present findings by performing DDI studies using PXB mice derived from the different hepatocyte donors.

Considering the magnitude of induction and its contribution to the drug metabolism in clinical situations, CYP3A4 is the most important enzyme to examine during the preclinical development of a new drug candidate. Several groups have established PXR and/or CYP3A4 humanized mice using gene knockout and transgenic techniques (Xie et al., 2000; Ma et al., 2007; Kim et al., 2008; Scheer et al., 2008; Hasegawa et al., 2011). On the other hand, the previous and present DDI studies have demonstrated that the induction of CYP2C enzymes also has a large impact on the pharmacokinetics of CYP2C substrate drugs (Niemi et al., 2003). At present, chimeric mice with a humanized liver, including the PXB mice, are only animal model available to investigate DDIs caused by the induction of CYP2C together with CYP3A4. Furthermore, several groups have reported that the drug-metabolizing profiles in PXB mice are similar to those in humans (Kamimura et al., 2010). Therefore, PXB mice seem to be a suitable animal model to examine the enzyme induction by a drug and its metabolite(s) if these are ligands for the human PXR. In conclusion, PXB mice will provide the opportunity to examine potential DDIs caused by PXR-related enzyme induction in a situation similar to that observed in humans.

Acknowledgments

We thank Tatsuya Matsumi and Dr. Saburo Sugai for supporting this research and reviewing the manuscript.

Authorship Contributions

Participated in research design: Hasegawa and Tahara.

Conducted experiments: Hasegawa, Tahara, Inoue, Kakuni, and Tateno.

Performed data analysis: Hasegawa.

Wrote or contributed to the writing of the manuscript: Hasegawa, Tahara, and Ushiki.

References

Chen Y and Goldstein JA (2009) The transcriptional regulation of the human CYP2C genes. *Curr Drug Metab* **10**:567–578.

Cui X, Thomas A, Gerlach V, White RE, Morrison RA, and Cheng KC (2008) Application and interpretation of hPXR screening data: validation of reporter signal requirements for prediction of clinically relevant CYP3A4 inducers. *Biochem. Pharmacol* **76**:680–689.

de Wildt SN, Kearns GL, Leeder JS, and van den Anker JN (1999) Cytochrome P450 3A: ontogeny and drug disposition. *Clin Pharmacokinet* **37**:485–505.

Dixit V, Hariparsad N, Li F, Desai P, Thummel KE, and Unadkat JD (2007) Cytochrome P450 enzymes and transporters induced by anti-human immunodeficiency virus protease inhibitors in human hepatocytes: implications for predicting clinical drug interactions. *Drug Metab Dispos* **35**:1853–1859.

Feng HJ, Huang SL, Wang W, and Zhou HH (1998) The induction effect of rifampicin on activity of mephenytoin 4′-hydroxylase related to M1 mutation of CYP2C19 and gene dose. *Br J Clin Pharmacol* **45**:27–29.

Hasegawa M, Kapelyukh Y, Tahara H, Seibler J, Rode A, Krueger S, Lee DN, Wolf CR, and Scheer N (2011) Quantitative prediction of human pregnane X receptor and cytochrome P450 3A4 mediated drug-drug interaction in a novel multiple humanized mouse line. *Mol Pharmacol* **80**:518–528.

Inoue T, Nitta K, Sugihara K, Horie T, Kitamura S, and Ohta S (2008) CYP2C9-catalyzed metabolism of 5-warfarin to 7-hydroxywarfarin in vivo and in vitro in chimeric mice with humanized liver. *Drug Metab Dispos* **36**:2429–2433.

Inoue T, Sugihara K, Ohshita H, Horie T, Kitamura S, and Ohta S (2009) Prediction of human disposition toward *S*-3H-warfarin using chimeric mice with humanized liver. *Drug Metab Pharmacokinet* **24**:153–160.

Jones SA, Moore LB, Shenk JL, Wisely GB, Hamilton GA, McKee DD, Tomkinson NC, LeCluyse EL, Lambert MH, Willson TM, et al. (2000) The pregnane X receptor: a promiscuous xenobiotic receptor that has diverged during evolution. *Mol Endocrinol* **14**:27–39.

Kamiguchi N, Aoyama E, Okuda T, and Moriwaki T (2010) A 96-well plate assay for CYP4503A induction using cryopreserved human hepatocytes. *Drug Metab Dispos* **38**:1912–1916.

Kamimura H, Nakada N, Suzuki K, Mera A, Sonda K, Murakami Y, Tanaka K, Iwatsubo T, Kawamura A, and Usui T (2010) Assessment of chimeric mice with humanized liver as a tool for predicting circulating human metabolites. *Drug Metab Pharmacokinet* **25**:223–235.

Kanebratt KP and Andersson TB (2008) HepaRG cells as an in vitro model for evaluation of cytochrome P450 induction in humans. *Drug Metab Dispos* **36**:137–145.

Kato M, Chiba K, Hisaka A, Ishigami M, Kayama M, Mizuno N, Nagata Y, Takakuwa S, Tsukamoto Y, Ueda K, et al. (2003) The intestinal first-pass metabolism of substrates of CYP3A4 and P-glycoprotein-quantitative analysis based on information from the literature. *Drug Metab Pharmacokinet* **18**:365–372.

Katoh M, Matsui T, Nakajima M, Tateno C, Soeno Y, Horie T, Iwasaki K, Yoshizato K, and Yokoi T (2005a) In vivo induction of human cytochrome P450 enzymes expressed in chimeric mice with humanized liver. *Drug Metab Dispos* **33**:754–763.

Katoh M, Watanabe M, Tabata T, Sato Y, Nakajima M, Nishimura M, Naito S, Tateno C, Iwasaki K, Yoshizato K, et al. (2005b) In vivo induction of human cytochrome P450 3A4 by rifabutin in chimeric mice with humanized liver. *Xenobiotica* **35**:863–875.

Kim S, Dinchuk JE, Anthony MN, Orcutt T, Zoeckler ME, Sauer MB, Mosure KW, Vuppugalla R, Grace JE Jr, Simmermacher J, et al. (2010) Evaluation of cynomolgus monkey pregnane X receptor, primary hepatocyte, and in vivo pharmacokinetic changes in predicting human CYP3A4 induction. *Drug Metab Dispos* **38**:16–24.

Kim S, Pray D, Zheng M, Morgan DG, Pezzano JG, Zoeckler ME, Chimalakonda A, and Sinz MW (2008) Quantitative relationship between rifampicin exposure and induction of Cyp3a11 in SXR humanized mice: extrapolation to human CYP3A4 induction potential. *Drug Metab Lett* **2**:169–175.

Kolars JC, Schmiedlin-Ren P, Schuetz JD, Fang C, and Watkins PB (1992) Identification of rifampin-inducible P450IIIA4 (CYP3A4) in human small bowel enterocytes. *J Clin Invest* **90**:1871–1878.

Lapple F, von Richter O, Fromm MF, Richter T, Thon KP, Wisser H, Griese EU, Eichelbaum M, and Kivistö KT (2003) Differential expression and function of CYP2C isoforms in human intestine and liver. *Pharmacogenetics* **13**:565–575.

LeCluyse EL (2001) Pregnane X receptor: molecular basis for species differences in CYP3A induction by xenobiotics. *Chem Biol Interact* **134**:283–289.

Luo G, Guenthner T, Gan LS, and Humphreys WG (2004) CYP3A4 induction by xenobiotics: biochemistry, experimental methods and impact on drug discovery and development. *Curr Drug Metab* **5**:483–505.

Ma X, Shah Y, Cheung C, Guo GL, Feigenbaum L, Krausz KW, Idle JR, and Gonzalez FJ (2007) The PREgnane X receptor gene-humanized mouse: a model for investigating drug-drug interactions mediated by cytochromes P450 3A. *Drug Metab Dispos* **35**:194–200.

Nakata K, Tanaka Y, Nakano T, Adachi T, Tanaka H, Kaminuma T, and Ishikawa T (2006) Nuclear receptor-mediated transcriptional regulation in Phase I, II, and III xenobiotic metabolizing systems. *Drug Metab Pharmacokinet* **21**:437–457.

Niemi M, Backman JT, Fromm MF, Neuvonen PJ, and Kivistö KT (2003) Pharmacokinetic interactions with rifampicin: clinical relevance. *Clin Pharmacokinet* **42**:819–850.

Niemi M, Backman JT, and Neuvonen PJ (2004) Effects of trimethoprim and rifampin on the pharmacokinetics of the cytochrome P450 2C8 substrate rosiglitazone. *Clin Pharmacol Ther* **76**:239–249.

Nishimura M, Koeda A, Morikawa H, Satoh T, Narimatsu S, and Naito S (2008a) Comparison of inducibility of multidrug resistance (MDR)1, multidrug resistance-associated protein (MRP)1, and MRP2 mRNAs by prototypical microsomal enzyme inducers in primary cultures of human and cynomolgus monkey hepatocytes. *Biol Pharm Bull* **31**:2068–2072.

Nishimura M, Koeda A, Shimizu T, Nakayama M, Satoh T, Narimatsu S, and Naito S (2008b) Comparison of inducibility of sulfotransferase and UDP-glucuronosyltransferase mRNAs by prototypical microsomal enzyme inducers in primary cultures of human and cynomolgus monkey hepatocytes. *Drug Metab Pharmacokinet* **23**:45–53.

Park JY, Kim KA, Kang MH, Kim SL, and Shin JG (2004) Effect of rifampin on the pharmacokinetics of rosiglitazone in healthy subjects. *Clin Pharmacol Ther* **75**:157–162.

Polk RE, Brophy DF, Israel DS, Patton R, Sadler BM, Chittick GE, Symonds WT, Lou Y, Kristoff D, and Stein DS (2001) Pharmacokinetic interaction between amprenavir and rifabutin or rifampin in healthy males. *Antimicrob Agents Chemother* **45**:502–508.

Raucy JL, Mueller L, Duan K, Allen SW, Strom S, and Lasker JM (2002) Expression and induction of CYP2C P450 enzymes in primary cultures of human hepatocytes. *J Pharmacol Exp Ther* **302**:475–482.

Scheer N, Ross J, Rode A, Zevnik B, Niehaves S, Faust N, and Wolf CR (2008) A novel panel of mouse models to evaluate the role of human pregnane X receptor and constitutive androstane receptor in drug response. *J Clin Invest* **118**:3228–3239.

Shin HC, Kim HR, Cho HJ, Yi H, Cho SM, Lee DG, Abd El Aty AM, Kim JS, Seo D, and Amadou GI (2009) Comparative gene expression of intestinal metabolizing enzymes. *Biopharm Drug Dispos* **30**:411–421.

Sinz M, Wallace G, and Sahi J (2008) Current industrial practices in assessing CYP450 enzyme induction: preclinical and clinical. *AAPS J* **10**:391–400.

Strom SC, Davila J, and Grompe M (2010) Chimeric mice with humanized liver: tools for the study of drug metabolism, excretion, and toxicity. *Methods Mol Biol* **640**:491–509.

Sugihara K, Kitamura S, Yamada T, Ohta S, Yamashita K, Yasuda M, and Fujii-Kuriyama Y (2001) Aryl hydrocarbon receptor (AhR)-mediated induction of xanthine oxidase/xanthine dehydrogenase activity by 2,3,7,8-tetrachlorodibenzo-p-dioxin. *Biochem. Biophys Res Commun* **281**:1093–1099.

Tateno C, Yoshizane Y, Saito N, Kataoka M, Utoh R, Yamasaki C, Tachibana A, Soeno Y, Asahina K, Hino H, et al. (2004) Near completely humanized liver in mice shows human-type metabolic responses to drugs. *Am J Pathol* **165**:901–912.

van de Kerkhof EG, de Graaf IA, Ungell AL, and Groothuis GM (2008) Induction of metabolism and transport in human intestine: validation of precision-cut slices as a tool to study induction of drug metabolism in human intestine in vitro. *Drug Metab Dispos* **36**:604–613.

Villikka K, Kivistö KT, Backman JT, Olkkola KT, and Neuvonen PJ (1997) Triazolam is ineffective in patients taking rifampin. *Clin Pharmacol Ther* **61**:8–14.

Xie W, Barwick JL, Downes M, Blumberg B, Simon CM, Nelson MC, Neuschwander-Tetri BA, Brunt EM, Guzelian PS, and Evans RM (2000) Humanized xenobiotic response in mice expressing nuclear receptor SXR. *Nature* **406**:435–439.

Zhou HH, Anthony LB, Wood AJ, and Wilkinson GR (1990) Induction of polymorphic 4′-hydroxylation of *S*-mephenytoin by rifampicin. *Br J Clin Pharmacol* **30**:471–475.

Address correspondence to: Dr. Maki Hasegawa, Kyowa Hakko Kirin Co., Ltd., 1188 Shimotogari, Nagaizumi-cho, Sunto-gun, Shizuoka, 411-8731, Japan. E-mail: maki.hasegawa@kyowa-kirin.co.jp

The American Journal of Pathology, Vol. 177, No. 2, August 2010

DOI: 10.2353/ajpath.2010.090430

Epithelial and Mesenchymal Cell Biology

Hepatic Hyperplasia Associated with Discordant Xenogeneic Parenchymal-Nonparenchymal Interactions in Human Hepatocyte-Repopulated Mice

Rie Utoh,*† Chise Tateno,*‡§ Miho Kataoka,* Asato Tachibana,*§ Norio Masumoto,*¶ Chihiro Yamasaki,*§ Takashi Shimada,§ Toshiyuki Itamoto,¶ Toshimasa Asahara,¶ and Katsutoshi Yoshizato*‡§‖**

From the Yoshizato Project, Cooperative Link of Unique Science and Technology for Economy Revitalization (CLUSTER), Hiroshima Prefectural Institute of Industrial Science and Technology, Hiroshima; the Institute of Advanced Biomedical Engineering and Science,† Tokyo Women's Medical University, Tokyo; the Hiroshima University Liver Project Research Center,‡ Hiroshima; PhoenixBio Co.,§ Hiroshima; the Department of Surgery,¶ Division of Frontier Medical Science, Graduate School of Biomedical Sciences, Hiroshima University, Hiroshima; Liver Research Center,‖ Osaka City University Graduate School of Medicine, Osaka; and the Department of Biological Science,** Developmental Biology Laboratory and Hiroshima University 21st Century COE Program for Advanced Radiation Casualty Medicine, Graduate School of Science, Hiroshima University, Hiroshima, Japan*

Liver mass is optimized in relation to body mass. Rat (r) and human (h) hepatocytes were transplanted into liver-injured immunodeficient mice and allowed to proliferate for 3 or 11 weeks, respectively, when the transplants stopped proliferating. Liver/body weight ratio was normal throughout in r-hepatocyte-bearing mice (r-hep-mice), but increased continuously in h-hepatocyte-bearing mice (h-hep-mice), until reaching approximately three times the normal m-liver size, which was considered to be hyperplasia of h-hepatocytes because there were no significant differences in cell size among host (mouse [m-]) and donor (r- and h-) hepatocytes. Transforming growth factor-β (TGF-β) type I receptor, TGF-β type II receptor, and activin A type IIA receptor mRNAs in proliferating r-hepatocytes of r-hep-mice were lower than in resting r-hepatocytes (normal levels) and increased to normal levels during the termination phase. Concomitantly, m-hepatic stellate cells began to express TGF-β proteins. In stark contrast, TGF-β type II receptor and activin A type IIA receptor mRNAs in h-hepatocytes remained low throughout and m-hepatic stellate cells did not express TGF-β in h-hep-mice. As expected, Smad2 and 3 translocated into nuclei in r-hep-mice but not in h-hep-mice. Histological analysis showed a paucity of m-stellate cells in h-hepatocyte colonies of h-hep-mouse liver. We conclude that m-stellate cells are able to normally interact with concordant r-hepatocytes but not with discordant h-hepatocytes, which seems to be at least partly responsible for the failure of the liver size optimization in h-hep-mice. *(Am J Pathol 2010, 177:654–665; DOI: 10.2353/ajpath.2010.090430)*

Experiments using animal models with damaged livers have demonstrated the high replicative potential of hepatocytes. A transgenic (Tg) mouse carrying an albumin (Alb) enhancer/promoter-driven murine urokinase-type plasminogen activator (uPA) gene was created[1]; the liver of this mouse degenerates and increases hepatocyte growth factor production and induces the proliferation of normal hepatocytes.[2] When transplanted into the uPA-Tg mice, mouse (m) hepatocytes engrafted into the host liver and proliferated, eventually replacing the host hepatocytes with a replacement index (RI) of 80%,[3] where RI represents the ratio of the regions occupied by transplanted hepatocytes in the host liver). The offspring generated by crossing uPA-Tg mice with immunodeficient mice were used as hosts for the xenotransplantation of rat (r),[4] woodchuck,[5] and human (h) hepatocytes.[6–8]

We showed that the repopulation kinetics of r-hepatocytes in uPA/severe combined immunodeficiency (SCID) mice were different from those of h-hepatocytes.[9] Rat

Supported in part by Cooperative Link of Unique Science and Technology for Economy Revitalization (CLUSTER), Promotion of Science and Technology in Regional Areas, Ministry of Education, Culture, Sports, Science and Technology, Japan.

Accepted for publication March 30, 2010.

None of the authors declare any relevant financial relationships.

Address reprint requests to Katsutoshi Yoshizato, Ph.D., PhoenixBio Co., Ltd., 3-4-1 Kagamiyama, Higashihiroshima, Hiroshima 739-0046, Japan. E-mail: katsutoshi.yoshizato@phoenixbio.co.jp.

hepatocytes rapidly proliferated and completely repopulated the mouse liver, whereas h-hepatocytes proliferated slowly over a longer period, with RI = ~90%. However, the livers of mice bearing h-hepatocytes (h-hep-mice) became much larger than the normal mass of the host mouse liver as the RI increased, whereas their counterparts with r-hepatocytes (r-hep-mice) did not (unpublished data). The above result with h-hep-mice does not meet the empirical rule (liver size optimization rule) that liver size is determined by the size of an animal's body.[10] This rule says that livers from smaller animals transplanted to larger animals must increase in size, which has been demonstrated in dogs,[10] humans,[11] and rats.[12]

Transforming growth factor (TGF)-β[13,14] and activin[15] are potent inhibitors of hepatocyte proliferation. The initiation of TGF-β signaling requires binding to the TGF-β type II receptor (TGFBR2), a constitutively active serine-threonine kinase, which subsequently *trans*-phosphorylates TGF-β type I receptor (TGFBR1). Activated TGFBR1 phosphorylates the Smad family proteins, Smad2 and 3 (Smad2/3), which then complex with Smad4 and translocate into the nucleus.[16] Smad2/3 are also activated by activin and nodal receptors, members of the TGF-β superfamily.[17] After partial hepatectomy, TGF-β mRNA expression increased in nonparenchymal cells, and TGF-β seemed to function as an inhibitory paracrine factor to prevent uncontrolled hepatocyte growth.[18]

When hepatocyte-targeted TGFBR2-knockout (KO) mice were subjected to 70% partial hepatectomy, hepatocytes grew beyond the limit of the known liver/body weight ratio ($R_{L/B}$),[19] supporting the antiproliferative role of TGF-β signaling. However, a similar study with hepatocyte-targeted TGFBR2-KO mice showed no significant differences in $R_{L/B}$ between control and KO mice because of an alternative increase in signaling via activin A/activin A type IIA receptor (ACVR2A) and persistent Smad pathway activity.[20] Thus, the roles of TGF-β, activin, and their receptors in the regulation of liver mass remain to be further studied.

In the present study, we compared the repopulation processes of concordant (rat) and discordant (human) xenogeneic hepatocytes in the uPA/SCID mouse liver. Our results showed that r-hep-mice had normal mouse regulation of $R_{L/B}$, whereas h-hep-mice underwent liver hyperplasia, resulting in the increase in $R_{L/B}$. The present study strongly suggests that discordant h-hepatocytes fail in exchanging molecular signals including TGF-β/activin with m-hepatic stellate cell (HSCs) and proliferate over the liver size optimization rule for mouse.

Materials and Methods

Preparation of Liver Tissues and Hepatocytes

The Hiroshima Prefectural Institute of Industrial Science and Technology Ethics Board approved this study. Liver tissues were obtained from seven donors in hospitals, with informed consent before the operations in accordance with the 1975 Declaration of Helsinki: four males, a 12-year-old male (12YM), a 28-year-old male (28YM), a 49-year-old male (49YM), and a 50-year-old male (50YM), and three females, a 25-year-old female (25YF), a 61-year-old female (61YF), and a 65-year-old female (65YF). The livers from the 25YF, 28YM, and 61YF were used for real-time RT-PCR to determine the expression levels of cell cycle-related genes and TGFBR/ACVR genes, and those from the 49YM, 50YM, and 65YF were used for immunostaining of proteins. Liver tissues were resected from 13-week-old male Fischer 344 rats (Charles River, Yokohama, Japan) and were used for real-time RT-PCR to determine the expression levels and immunohistochemistry.

h-Hepatocytes were isolated from the 12YM as reported previously.[7,21] Cryopreserved h-hepatocytes from two males, a 9-month-old male (9MM) and a 13-year-old male (13YM), were obtained from In Vitro Technologies (Baltimore, MD); h-hepatocytes from a 10-year-old female (10YF) were purchased from BD Biosciences (San Jose, CA). The hepatocytes from these four donors were used for transplantation experiments into uPA/SCID mice. r-Hepatocytes were isolated from the livers of Fischer 344 rats by collagenase perfusion,[22] centrifuged through 45% Percoll at 50 $\times$ *g* for 24 minutes and used for transplantation experiments. These hepatocyte preparations all showed >80% of viability, which was determined by the dye extrusion test, and >99% of purity, which was determined by microscopic observation.

Transplantation of Hepatocytes

h- and r-Hepatocytes, 7.5×10^5 and 5×10^5 cells, respectively, were transplanted into the liver of homozygous uPA/SCID mice, which had been generated by crossing uPA-Tg mice with SCID mice.[7] Donor h-hepatocytes showed reproducibly high engraftment efficiency similar to fresh r-hepatocytes and RI >80% under the optimized conditions. The labeling index (LI) of 5-bromo-2′-deoxyuridine (BrdU) of the transplanted hepatocytes was determined as a measure of DNA synthesis by exposing the host animals to BrdU for 1 hour before sacrifice.[23]

Histochemistry

Paraffin and frozen sections of 5-μm thickness were prepared from liver tissues as detailed previously.[7,23] The sections were stained with H&E or subjected to immunohistochemical analysis using the primary antibodies listed in Table 1 together with necessary information. For bright-field immunohistochemistry, the antibodies were visualized with the VECTASTAIN ABC kit (Vector Laboratories, Burlingame, CA) using 3,3′-diaminobenzidine as the substrate. The sections were counterstained with Mayer's hematoxylin. Fluorescent immunohistochemistry was performed using Alexa 488- or 594-conjugated donkey anti-mouse IgG or donkey anti-rabbit IgG (Invitrogen) as secondary antibodies and then with Hoechst 33258 for nuclear staining. Human cytokeratin 8/18 (hCK8/18) antibodies reacted with h-hepatocytes but not with m-hepatocytes. Rat major histocompatability complex class I RT1A (rRT1A) antibodies reacted with r-hepatocytes but not with m-hepatocytes. The RIs of h- and r-hepatocytes ($RI_{h\text{-}hep}$ and $RI_{r\text{-}hep}$, respectively) were calculated as the ratios of the

Table 1. Antibodies for Immunohistochemical Analysis

Antibodies	Clone (clone name)	Host	Dilution	Fixation	Sections	Supplier
Human CK8/18*	Monoclonal (NCL 5D3)	Mouse	50	Aceton	Frozen	MP Biomedicals (Aurora, OH)
Human albumin* (cross-adsorbed)	Polyclonal	Goat	200	Formalin	Paraffin	Bethyl Laboratories (Montgomery, TX)
BrdU	Monoclonal (Bu20a)	Mouse	50	Formalin	Paraffin	DAKO (Glostrup, Denmark)
Rat RT1A†	Monoclonal (OX-18)	Mouse	100	Aceton	Frozen	Chemicon International (Temecula, CA)
Mouse type IV collagen	Polyclonal	Rabbit	500	Aceton	Frozen	LSL (Tokyo, Japan)
Human MRP2‡	Polyclonal	Rabbit	200	Aceton	Frozen	Sigma (St. Louis, MO)
Human TGFBR2§	Polyclonal	Rabbit	500	Aceton	Frozen	Upstate (Billerica, MA)
TGF-β1¶	Polyclonal	Rabbit	10	Formalin	Frozen	BioVision (Mountain View, CA)
Human desmin§	Monoclonal	Mouse	50	Formalin	Frozen	DAKO
Human Smad2§	Polyclonal	Rabbit	50	Non-fixed	Frozen	Zymed Laboratories (South San Francisco, CA)
Human Smad3§	Polyclonal	Rabbit	200	Formalin	Paraffin	Zymed Laboratories
Human E-cadherin§	Polyclonal	Rabbit	200	Formalin	Frozen	Abcam (Cambridge, MA)

*Human-specific antibody.
†Rat-specific antibody.
‡Cross-reactive with rat antigen.
§Cross-reactive with rat and mouse antigens.
¶Cross-reactive with TGF-β1-3.

area occupied by hCK8/18$^+$ h-hepatocytes and the area occupied by rRT1A$^+$ r-hepatocytes to the entire area examined on immunohistochemical sections from six lobes, respectively, as described previously.[7] BrdU LIs of h- and r-hepatocytes ($LI_{h\text{-}hep}$ and $LI_{r\text{-}hep}$, respectively) were calculated as the ratios of BrdU$^+$ nuclei to hAlb$^+$ h-hepatocytes and rRT1A$^+$ r-hepatocytes, respectively, in 10 randomly selected fields from three different lobes.

A transferase-mediated dUTP nick end-labeling (TUNEL) assay was performed as follows. Paraffin-embedded liver tissues were sectioned, deparaffinized, and subjected to TUNEL analysis using an ApopTag Peroxidase In Situ Apoptosis Detection Kit (Chemicon International, Temecula, CA) following the manufacturer's instructions.

Real-Time RT-PCR

Total RNA was isolated from normal and chimeric liver tissues using Isogen (Nippon Gene, Tokyo, Japan) and aliquots, 1 μg each, were reverse-transcribed with random hexamers using PowerScript Reverse Transcriptase (Clontech, Kyoto, Japan). The expressions of the following genes were measured by real-time RT-PCR using an SYBR Green PCR Master Mix (Applied Biosystems, Foster City, CA) in an ABI Prism 7700 sequence detector (Applied Biosystems): h-forkhead box M1 (hFoxM1), h-cyclin dependent kinases (hCdk) 1, hCyclin B1, hCyclin D1, h-cell division cycle 25A (hCdc25A), hTGFBR1, hTGFBR2, hACVR2A, h-glyceraldehyde 3-phosphate dehydrogenase (hGAPDH), rat TGFBR1 (rTGFBR1), rTGFBR2, rACVR2A, and rGAPDH. The gene-specific primers we used are shown in Table 2. These primers correctly amplified the corresponding human/rat genes but not the mouse genes. The relative mRNA expressions of transplanted h- and r-hepatocytes were quantified using the comparative threshold cycle ($\Delta\Delta C_T$) method[24] according to the manual provided by Applied Biosystems. hGAPDH and rGAPDH, respectively, were used as the internal reference genes to normalize the expression of human/

Table 2. Primer Sets for Real-Time RT-PCR

Gene	Forward primer	Reverse primer
hFoxM1	5′-GCATCTACTGCCTCCCTGTG-3′	5′-GAGGAGTCTGCTGGGAACG-3′
hCdk1	5′-AAACTACAGGTCAAGTGG-3′	5′-GGGATAGAATCCAAGTATTTCTTCAG-3′
hCyclin B1	5′-CCTGATGGAACTAACTATGTTG-3′	5′-CATGTGCTTTGTAAGTCCTTGA-3′
hCyclin D1	5′-TGTGAAGTTCATTTCCAATCCG-3′	5′-CTGGAGAGGAAGCGTGTGAG-3′
hCdc25A	5′-CAAAGAGGAGGAAGAGCATGTC-3′	5′-CCAGGGATAAAGACTGATGAAGAG-3′
hTGFBR1	5′-GGAATTCATGAAGATTACCAAC-3′	5′-AGAGTTCAGGCAAAGCTGTAGA-3′
hTGFBR2	5′-CATGTGTTCCTGTAGCTCTGAT-3′	5′-TGCCGGTTTCCCAGGTTGA-3′
hACVR2A	5′-AAGAAGACCCTTTGTTGAAAAATG-3′	5′-GCAAGGTTTCTCTTAGTCTCATGTC-3′
hSmad2	5′-AAAGCTTCACCAATCAAGTCC-3′	5′-CTTCTCTTCCTCTTTAATGGG-3′
hSmad3	5′-TGGAACTCTACTCAACCCAT-3′	5′-GGTAAATGTGTTTGGCAGAC-3′
hGAPDH	5′-ACCAGGGCTGCTTTTAACTC-3′	5′-ATTGATGACAAGCTTCCCG-3′
rTGFBR1	5′-CACTTCTGATTCCCACTCTTG-3′	5′-ATGAAGGAGCAGGAGCTGTA-3′
rTGFBR2	5′-CAAGTCGGTTAACAGCGAT-3′	5′-GGCTTCTCACAGATGGAGG-3′
rACVR2A	5′-AGCATGGATTGGGAGACTTC-3′	5′-GCCACATTCTTCGTGTAAGTT-3′
rGAPDH	5′-CCAGGGCTGCCTTCTCTTGTGA-3′	5′-GCCGTTGAACTTGCCGTGGGTA-3′

h, human-specific; r, rat-specific.

rat target genes; h/r-specific primers were used because there is a difference in the amounts of h/r-cDNAs in the mixed baths from the h- or r-hep-mouse liver. Before performing quantification with the $\Delta\Delta C_T$ method, we confirmed that the amplification efficiencies of target and reference primers were approximately equal. The expression levels of the target genes show the relative differences from the normal h/r-liver controls. For all data, the h/r target C_T value was normalized using the formula: $\Delta C_T = C_T$ h/r target $- C_T$ h/rGAPDH. To determine the relative expression levels, the formula, $\Delta\Delta C_T = \Delta C_T$ sample (chimeric livers) $- \Delta C_T$ calibrator (h/r-livers), was used and $2^{-\Delta\Delta C_T}$ was plotted.

Statistics

Results are shown as the mean ± SD. Significant differences between groups were detected with Dunnett's multiple comparison test or Student's *t*-tests using StatView software (SAS Institute Japan, Tokyo, Japan).

Results

Growth Kinetics for r- and h-Hepatocytes in uPA/SCID Mice

Twelve mice were transplanted with r-hepatocytes and sacrificed at 1, 2, 3, and 4 weeks after transplantation. Liver sections were subjected to double immunostaining for BrdU and rRT1A to determine the $LI_{r\text{-}hep}$ and the $RI_{r\text{-}hep}$ (Figure 1A), where $LI_{r\text{-}hep}$ represents the ratio of the BrdU-positive r-hepatocyte number to the total r-hepatocytes in the r-hepatocyte-repopulated region in the r-hep-mouse liver, and $RI_{r\text{-}hep}$ represents the ratio of the repopulated r-hepatocytes to the total r- and m-hepatocytes in the r-hep-mouse liver. $LI_{r\text{-}hep}$ was approximately 15% at 1 week, when $RI_{r\text{-}hep}$ was approximately 7%. $RI_{r\text{-}hep}$ reached almost 100% at 3 weeks when $LI_{r\text{-}hep}$ had markedly decreased to 1%. Finally, $LI_{r\text{-}hep}$ returned to the control level (0.4%) at 4 weeks, the level of LI of SCID mouse liver. From these results, we concluded that r-hepatocytes terminated proliferation at approximately 3 weeks.

Mice were transplanted with h-hepatocytes isolated from the 9MM ($h\text{-}hep_{9MM}$) and were sacrificed at 1 to 11 weeks after transplantation (Figure 1B). $LI_{h\text{-}hep}$ and $RI_{h\text{-}hep}$, the corresponding ratios for h-hep-mouse liver, were approximately 10% and <1% at 1 week, respectively. The $LI_{h\text{-}hep}$ at this time period was 64% of the $LI_{r\text{-}hep}$. The rise of $RI_{h\text{-}hep}$ and the decrease of $LI_{h\text{-}hep}$ thereafter were both greatly slow compared with those of the r-hep-mice. $LI_{h\text{-}hep}$ returned to the control level at 11 weeks when $RI_{h\text{-}hep}$ was still as low as 58 ± 46%. Thus, it was concluded that h-hepatocytes repopulate the m-liver quite slowly. We believe that this difference in donor proliferative and repopulating activities is due to species-related differences but not experimental variables that might influence transplantation outcomes, because, first, the engraftment efficiencies were similar between the h- and the r-hepatocytes, second, the viability (>80%) and the purity (>99%) of the hepatocyte preparations were comparable between the two types of hepatocytes, and, third, the similar difference was observed

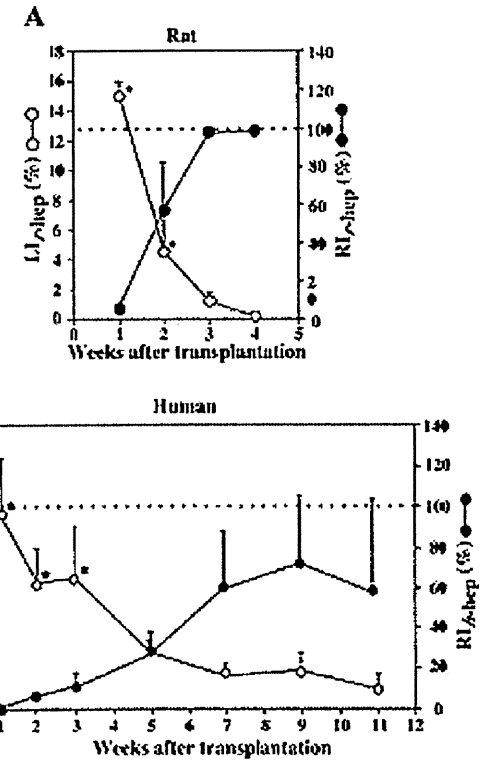

Figure 1. Repopulation of r- and h-hepatocytes in mice. uPA/SCID mice were transplanted with r-hepatocytes (**A**) and h-hepatocytes (**B**) and sacrificed at the indicated times (weeks) after transplantation. **A:** r-hep-Mice. Histological sections were prepared from three different lobes and stained for rRT1A and BrdU. $rRT1A^+$ and $BrdU^+$ double-positive hepatocytes and $rRT1A^+$ hepatocytes were counted to determine $LI_{r\text{-}hep}$ (open circle) and $RI_{r\text{-}hep}$ (closed circle), respectively. **B:** $h\text{-}hep_{9MM}$-Mice. $LI_{h\text{-}hep}$ (open circle) and $RI_{h\text{-}hep}$ (closed circle) were similarly determined, except that h-hepatocytes were identified using hAlb antibodies. The LI of livers taken from control animals (8- to 15-week-old SCID mice) was 0.4 ± 0.2% ($n = 3$). Significant differences compared with normal livers (*$P < 0.05$). The dotted horizontal line indicates RI = 100%.

in the previous report in which h-hepatocytes were also used as donor hepatocytes.[9]

Information regarding proliferative activity of h-hepatocytes was obtained by determining the gene expression levels of five cell cycle promotion genes (hCdk1, hCyclin B, hFoxM1, hCdc25A, and hCyclin D) in the h-hep-mouse livers during repopulation, together with those in normal h-livers from three donors. The results are shown as the relative mRNA expression levels against those in the normal h-livers (Figure 2). h-hep-Mouse livers expressed hCdk1 and hCyclin B1 at much and moderately higher levels at 3 to 9 weeks, respectively. The expressions of hFoxM1 and hCdc25A were significantly higher in h-hep-mouse livers up to 7 weeks. These genes all reduced the expression to levels comparative to normal h-liver levels at 11 weeks. These results indicate that h-hepatocytes in h-hep-mice terminated growth at 11 weeks after transplantation.

Correlation of $R_{L/B}$ with RI in h-Chimeric Mice

In the experiments shown in Figure 1, we noticed that the h-hep-mouse liver enlarged beyond the normal volume of

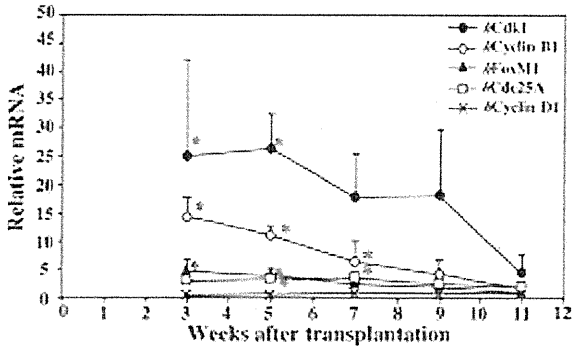

Figure 2. Expressions of cell cycle-related genes during h-hepatocyte repopulation in h-hep-mice. h-hep-Mouse livers were removed at 3 to 11 weeks after transplantation from h-hep-mice shown in Figure 1B and subjected to real-time RT-PCR for hCdk1 (closed circle), hCyclin B1 (open circle), hFoxM1 (closed triangle), hCdc25A (open square), and hCyclin D1 (×). Gene expressions were also determined for normal human livers from the 25YF, 28YM, and 61YF donors. Gene expressions were all normalized to hGAPDH expression. The ratio of mRNA expression for each gene in h-hep-mouse livers was calculated by dividing the normalized value of each gene of h-hep-mouse livers by the normalized value of corresponding gene of the normal h-livers. The ratios are plotted against weeks after transplantation. The variation of each gene of the normal livers was 1.0 ± 0.3, 1.0 ± 0.6, 1.0 ± 0.4, 1.0 ± 0.5, and 1.0 ± 0.3 for hFoxM1, hCdk1, hCyclin B1, hCyclin D1, and hCdc25A, respectively. Significant differences against normal h-livers (*$P < 0.05$).

the host liver as $RI_{h\text{-}hep}$ increased. We assessed a correlation between $RI_{h\text{-}hep}$ and liver mass during h-hepatocyte repopulation. A total of 38 h-hep-mice were generated using h-hepatocytes from three donors (9MM, 12YM, and 13YM) and were sacrificed at 11 to 14 weeks after transplantation. No significant increase in blood hAlb levels was observed at 9 to 10 weeks, indicating that the livers then had entered the termination phase of growth, which is consistent with the results shown in Figure 2. Host liver and body weights were measured at sacrifice to calculate $R_{L/B}$. Liver sections were prepared from each mouse and stained for hCK8/18 to determine RI. $R_{L/B}$ was then plotted against RI (Figure 3A). $R_{L/B}$ increased as RI increased, with a correlation coefficient (r^2) of 0.59. The gross appearances of the selected h-hep-mouse livers are shown in Figure 3, B–D. Livers of an h-hep-mouse with RI = 0% showed $R_{L/B}$ = 6.9 ± 1.0% (Figure 3, A and B). Twenty of the 38 h-hep-mice showed RI >50%. Five h-hep-mice showed RIs >80%, one of which had $R_{L/B}$ = 11.8% and is shown in Figure 3C. The highest RI was 92.1%, which was obtained in a chimeric $h\text{-}hep_{9MM}$ mouse with $R_{L/B}$ = 19.3% (Figure 3D). The $R_{L/B}$ for the five mice with RIs >80% was 13.2 ± 3.5%, which was >2-fold of the value at the time of transplantation (6.0 ± 1.1%, n = 4) or that (5.4 ± 0.5%, n = 3) observed in SCID mice (Figure 3A). Importantly, the $R_{L/B}$ of r-hep-mice did not change during repopulation (Figure 3E, 5 weeks) and was similar to that of SCID mice (5.4 ± 0.5%, n = 3): $R_{L/B}$ = 6.5 ± 1.1, 6.3 ± 0.2, 6.4 ± 0.2, and 5.8 ± 0.2% (each n = 3), at 2, 3, 4, and 5 weeks after transplantation, when RIs were 57.1 ± 24.7, 97.1 ± 3.0, 98.6 ± 2.4, and 100 ± 0.0%, respectively. This fact suggests that the increase in r-hepatocyte number and the death of injured m-hepatocytes are normally balanced in the r-hep-mouse liver. However, $R_{L/B}$ of h-hep-mice increased as the RI increased as above, suggesting a possible

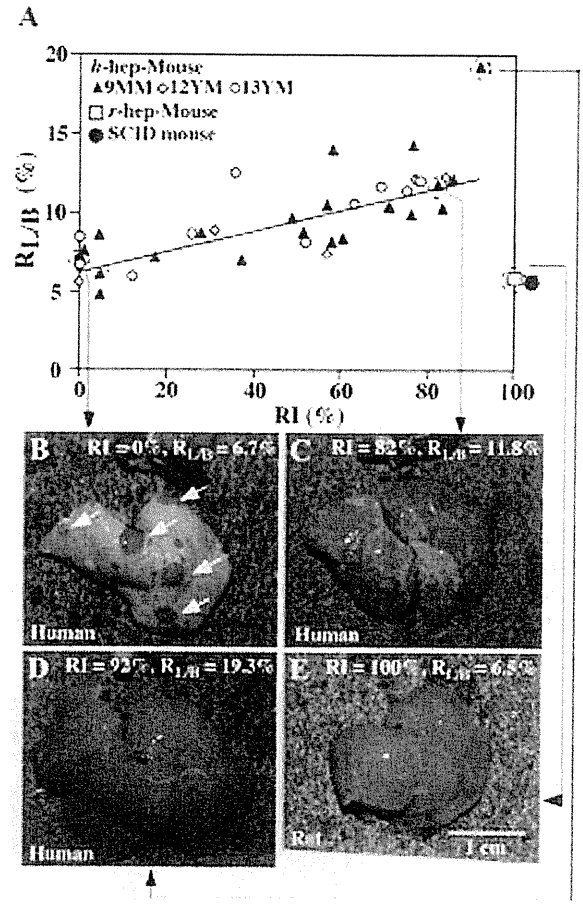

Figure 3. Correlation of $R_{L/B}$ with RI in h-hep-mice. **A:** Twenty-one, 6, and 11 h-hep-mice were produced by transplanting hepatocytes from the 9MM, 12YM, and 13YM donors, respectively, and then sacrificed at 11 to 14 weeks after transplantation. $R_{L/B}$ and RI were determined at sacrifice and plotted together. Closed triangle, 9MM hepatocytes; open diamond, 12YM hepatocytes; open circle, 13YM hepatocytes. Four r-hep-mice were produced and sacrificed at five weeks after transplantation when the repopulation had completed, and $R_{L/B}$ and RI were determined (open square). $R_{L/B}$ was also determined for three 8- to 15-week-old SCID mice (closed circle). **B–D:** Gross appearances of h-hep-mouse livers at 11 weeks. The four **long arrows** in the figure starting from each of mouse symbols in **A** point to the photos of the corresponding mouse livers shown in **B**, **C**, **D**, and **E**, respectively. **B:** The liver of an $h\text{-}hep_{9MM}$ mouse with RI = 0% and $R_{L/B}$ = 6.7%. **Arrows** indicate reddish colonies of m-hepatocytes that deleted the transgene. Whitish regions are occupied by Tg host hepatocytes. The dark red-colored organ placed above the liver is spleen removed from the same recipient. **C:** The liver of an $h\text{-}hep_{9MM}$ mouse with RI = 82% and $R_{L/B}$ = 11.8%. **D:** The liver of an $h\text{-}hep_{9MM}$ mouse with RI = 92% and $R_{L/B}$ = 19.3%. **E:** The liver of an r-hep-mouse with RI = 100% and $R_{L/B}$ = 6.5%. Scale bar = 1 cm.

imbalance between h-hepatocyte proliferation and m-hepatocyte death.

To test this possibility we performed the TUNEL analysis and determined the ratios (%) of the TUNEL$^+$ (dead) m-hepatocytes during the repopulation of h-hepatocytes as follows: 0.5 ± 0.1, 0.6 ± 0.2, 1.2 ± 0.1, 0.6 ± 0.3, 0.2 ± 0.1, 3.9 ± 4.7, and 8.5 ± 6.8 at 1, 2, 3, 5, 7, 9, and 11 weeks (each n = 3), respectively. The ratios were quite low until 7 weeks after transplantation and were much lower than those of the BrdU$^+$ h-hepatocytes shown in Figure 1B (~10% at 1 week and ~2% at 7 weeks). Similar TUNEL analysis showed a TUNEL$^+$ ratio of 18.8 ± 6.1% (n = 3) for r-hep-mice at 3 weeks after transplantation, which is con-

siderably higher than that of h-hep-mice at 3 weeks (1.2 ± 0.1%). Based on these analyses, we concluded that the proliferation rate of h-hepatocytes is higher than the death rate of m-hepatocytes, which resulted in the enlargement of liver in h-hep-mice.

Histological Architecture of Sinusoids and Bile Canaliculi in Chimeric Mouse

Liver sinusoids were histologically examined, because their structures reflect the proliferation status of hepatocytes: their structures are compressed[25] and become vague[26] during vigorous hepatocyte proliferation. r-hep- and h-hep$_{9MM}$ Mice were generated and sacrificed in the proliferation (at 2 and 5 weeks after transplantation for r-hep- and h-hep$_{9MM}$ mice, respectively) and proliferation termination phases (at 5 and 14 weeks for r-hep- and h-hep$_{9MM}$ mice, respectively) for histological analysis (Figure 4). Normal livers from Fischer 344 rats and the 65YF donor were used as normal r- and h-liver controls, respectively. H&E sections clearly showed the single-cell structures of hepatic plates in normal r-livers (Figure 4A)

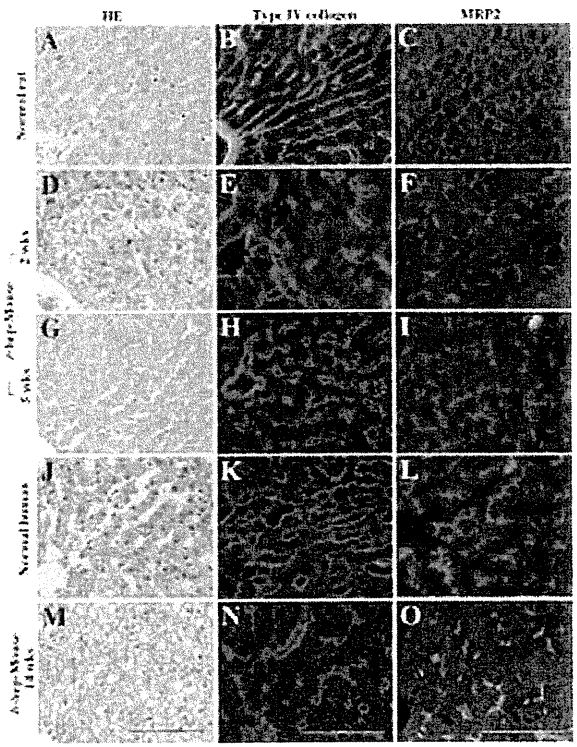

Figure 4. Histological characteristics of r-hep- and h-hep-mouse livers. Normal r- and h-livers were obtained from 13-week-old male Fischer 344 rats (**A–C**) and from a 65YF donor (**J–L**), respectively. r-hep-Mice and h-hep-mice were produced as shown in Figure 1. The former were sacrificed at two (proliferation phase, **D–F**) and five weeks (wks) after transplantation (termination phase, **G–I**) and the latter at 14 weeks (termination phase, **M–O**). Liver sections were stained with H&E (**A**, **D**, **G**, **J**, and **M**) and for type IV collagen (red, **B**, **E**, **H**, **K**, and **N**) and MRP2 (red, **C**, **F**, **I**, **L**, and **O**). The sections from rats and r-hep-mice were additionally stained for rRT1A (green, **B**, **C**, **E**, **F**, **H**, and **I**) and those from the human and h-hep-mice for hCK8/18 (green, **K**, **L**, **N**, and **O**) to identify transplanted r- and h-hepatocytes, respectively. The dashed line in **D** shows the boundary between r-hepatocyte (*r*) and m-hepatocyte regions (*m*). Scale bar = 100 μm.

and h-livers (Figure 4J). Sections were stained for type IV collagen, an indicator of the subsinusoidal space,[26] and multidrug resistance-associated protein 2 (MRP2), a maker of the canalicular organic anion transporters.[27] These proteins were localized as expected in normal r-livers (Figure 4, B and C) and h-livers (Figure 4, K and L).

H&E-stained sections from r-hep- and h-hep-mouse livers at 5 and 14 weeks, respectively, showed complete repopulation (Figure 4, G and M, respectively), but their histological features were quite different. h-Hepatocytes were less eosinophilic than r-hepatocytes, as reported previously,[7] and swollen and contained less cytoplasm, with wisps of accumulated glycogen, as described previously.[8] Single-cell plates were rarely observable in the

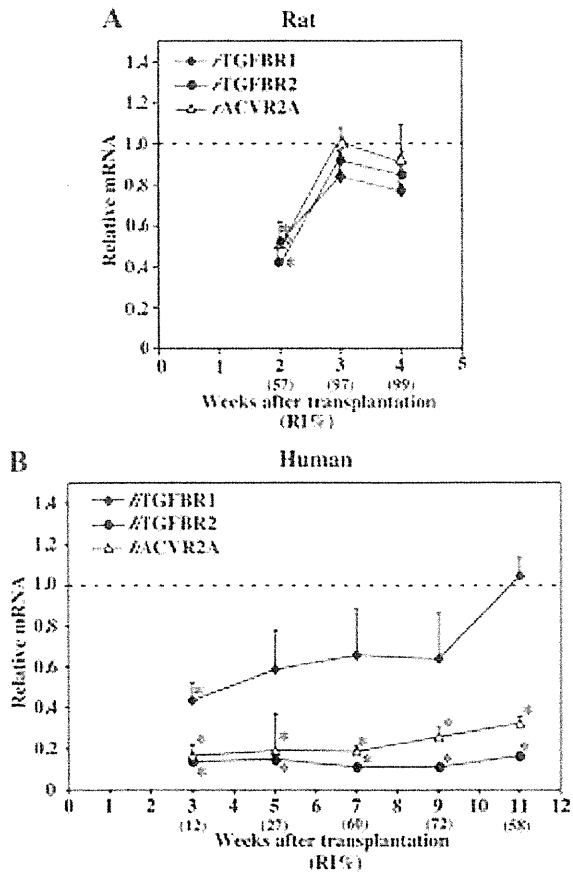

Figure 5. Gene expressions of TGFBR1, TGFBR2, and ACVR2A in r-hep- and h-hep-mouse livers. Real-time RT-PCR was performed by using total mRNA isolated from the livers of r-hep- and h-hep$_{9MM}$ mice shown in Figure 1 as templates, and each result was normalized to that of rGAPDH and hGAPDH. Likewise real-time RT-PCR was performed for liver tissues from 13-week-old male rats and those from the 25YF, 28YM, and 61YF human donors as the normal rat and human controls, respectively. mRNA abundance in r- and h-chimeric mice was divided by that of the normal r- and h-livers, respectively, and is shown as relative mRNA abundance (ordinary axis) in **A** for r-hep-mice and in **B** for h-hep-mice. Normal livers in **A** were obtained from three 13-week-old male rats and those in **B** from three donors, 25YF, 28YM, and 61YF. The dotted horizontal lines show the average expression level in normal livers (1.0). The variations of the normalized rTGFBR1, rTGFBR2, rACVR2, hTGFBR1, hTGFBR2, and hACVR2 were 1.0 ± 0.2, 1.0 ± 0.2, 1.0 ± 0.2, 1.0 ± 0.2, 1.0 ± 0.4, and 1.0 ± 0.2, respectively. Values represent the mean ± SD (n = 3). Significant differences compared with normal livers ($^*P < 0.05$). "RI%" shows the average RI calculated from three mice. Closed diamond, TGFBR1; closed circle, TGFBR2; and open triangle, ACVR2A.

h-hepatocyte-regions in h-hep-mice at 14 weeks (Figure 4M), and sinusoids were obscure. Type IV collagen immunostains demonstrated multicell-layer-thick hepatic plates (Figure 4N). The MRP2 protein was randomly distributed in the intercellular space (Figure 4O). Similar histological structures were observed in the h-hepatocyte regions at 5 weeks (data not shown). Likewise sinusoidal structures were not distributed in an orderly fashion in the r-hepatocyte regions of r-hep-mice at 2 weeks when r-hepatocytes were in the proliferation phase (Figure 4, D–F), losing vessel continuity along the portal-central axis. However, r-hep-mice at 5 weeks after transplantation regained the normal arrangement of hepatic plates and sinusoids (Figure 4G), which was consistent with the distributions of type IV collagen and MRP2 (Figure 4, H and I). These proteins were located as in normal r-liver, indicating the reconstruction of the resting liver structure with single hepatic plates along the portal-central axis. These results demonstrate that the h-hepatocytes were incapable of reconstructing the resting liver structure even at 14 weeks after transplantation.

The length of the long axis of hepatocytes was determined on H&E-stained sections from r- and h-hep-mice shown in Figure 4 as a measure of size, which showed no significant differences among m (host)-, r-, and h-hepatocytes in chimeric livers: uPA-expressing m-hepatocytes in h-hep$_{9MM}$ mice at 11 weeks after transplantation, 19.5 ± 4.5 μm (n = 3); uPA-expressing m-hepatocytes in r-hep-mice at 2 weeks, 19.7 ± 4.3 μm (n = 3); r-hepatocytes in r-mice at 5 weeks, 22.7 ± 2.9 μm (n = 3); and h-hepatocytes in h-hep-mice at 11 to 14 weeks, 22.5 ± 1.8 μm (n = 6). This result clearly indicated that the observed enlargement of the h-hep-mouse liver was caused by hyperplasia but not hypertrophy of h-hepatocytes.

TGF-β Signaling in r-hep- and h-hep-Mouse Livers

TGF-β and activin play active roles in the termination of liver regeneration.[14,15,18–20,28] The mRNA expressions of TGFBR1, TGFBR2, and ACVR2A were determined in r-hep-mouse livers at 2, 3, and 4 weeks after transplantation and in h-hep$_{9MM}$ mouse livers at 3, 5, 7, 9, and 11 weeks and compared with those of normal r- and h-liver controls, respectively. In r-hep-mice at 2 weeks (proliferation phase, RI$_{r\text{-}hep}$ = 57%), rTGFBR1, rTGFBR2, and rACVR2A expressions were suppressed to half those of normal r-livers and gradually returned to normal levels at 3 and 4 weeks (termination phase, RI$_{r\text{-}hep}$ = 97 and 99%,

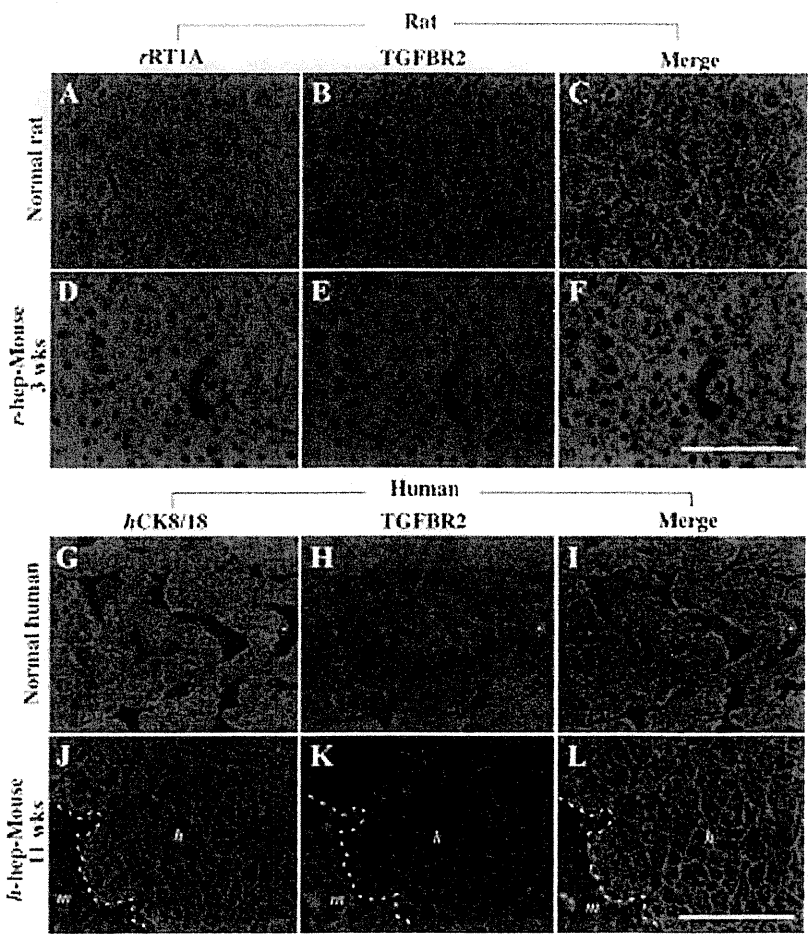

Figure 6. Identification and distribution of TGFBR2 in normal and chimeric livers. uPA/SCID mice were transplanted with r- and h-hepatocytes$_{9MM}$ and sacrificed at 3 and 11 weeks after transplantation, respectively, when the transplanted hepatocytes had terminated proliferation. Two series of double immunohistochemical examinations were performed on liver tissues, one for rat series (Rat) shown in **A–F** that contained normal r-liver (Normal rat) shown in **A–C** and r-hep-mouse liver (**D–F**) and the other for the human series (Human) shown in **G–L** that contained 9MM donor liver as control normal h-liver (Normal human, **G–I**) and h-hep-mouse liver (**J–L**). Liver sections of rat series were double-stained for rRT1A for identifying r-hepatocytes (green; **A** and **D**) and TGFBR2 (red; **B** and **E**) and those of human series for hCK8/18 for identifying h-hepatocytes (green; **G** and **J**) and TGFBR2 (red; **H** and **K**). Images **A** and **B**, **D** and **E**, **G** and **H**, and **J** and **K** were merged and are shown in **C**, **F**, **I**, and **L**, respectively. Similar staining results were obtained from three different mice of each series. The **dashed lines** in **J–L** indicate the boundary between h-hepatocyte (*h*) and m-hepatocyte regions (*m*). Scale bar = 100 μm.

respectively) (Figure 5A) as reported in the regeneration of partial hepatectomized r-liver.[29] In contrast, their expression profiles in h-hep-mouse livers were quite different (Figure 5B). At 3 weeks (proliferation phase, $RI_{h\text{-}hep}$ = 12%), hTGFBR2 and hACVR2A were expressed at levels less than one-third of normal levels; expression remained low throughout the 11-week-long observation period. The suppression of the expression of these genes was reproducible, because similar results were obtained from h-hep-mice generated with another donor (10YF): the ratios of expression levels of hTGFBR2 and hACVR2A in the h-hep-mice at 9 to 11 weeks after transplantation to those in the normal human livers were 0.19 ± 0.05 (n = 3) and 0.19 ± 0.02 (n = 3), respectively. The expression of hTGFBR1 mRNA was high compared with that of these two mRNAs at 3 weeks and gradually increased until reaching the normal levels at 11 weeks.

The expression of TGF-β receptor, TGFBR2, was immunohistochemically examined in r- and $h\text{-}hep_{3MM}$ mouse livers at 3 and 11 weeks when the mice showed RI = 97 ± 3% (n = 3) and 58 ± 46% (n = 3), respectively, together with staining for rRT1A and hCK8/18 to identify r- and h-hepatocytes, respectively (Figure 6). As with normal r-hepatocytes (Figure 6, A–C), the $rRT1A^+$ r-hepatocytes in r-hep-mice were stained heavily for TGFBR2 (Figure 6, D–F). Likewise normal h-hepatocytes abundantly expressed TGFBR2 (Figure 6, G–I). In contrast, TGFBR2 was hardly detectable in $hCK8/18^+$ h-hepatocytes in h-hep-mice (Figure 6, J–L). The anti-TGFBR2 antibody used was cross-reactive with r- and m-TGFBR2. The $TGFBR2^+$ cells in the m-hepatocyte region seen in Figure 6K were largely m-hepatocytes according to their morphology. Moderately $TGFBR2^+$ cells in the h-hepatocyte region shown in Figure 6K were mostly m-nonparenchymal cells and few h-hepatocytes (Figure 6, K and L). These results indicated that h-hepatocytes in h-hep-mice maintain low sensitivity tc TGF-β, although the expression of TGFBR1 was up-regulated at 11 weeks after transplantation. It is known that TGF-β initially binds to TGFBR2, and TGF-β signals are transferred through the heterodimers of TGFBR1 and TGFBR2.[16] TGF-β-expressing cells were identified in liver sections from r- and h-hep-mice during the proliferation and termination phases by double-immunostaining for desmin and TGF-β (Figure 7). Compared with the control (Figure 7, A–C; normal liver from wild-type SCID mice), tissues collected from the injured livers of uPA/SCID mice contained abundant $desmin^+$ HSCs that were all heavily expressing TGF-β (Figure 7, D–F) as reported previously.[2] Very few $desmin^+$ cells were observed in r-hep-mice at 2 weeks (Figure 7, G–I) or in h-hep-mice at 5 weeks (Figure 7, M–O), suggesting that very few m-HSCs invaded the xenogeneic hepatocyte colonies during the proliferation phase. These cells were all $TGF\text{-}\beta^-$. m-HSCs increased in number in xenogeneic hepatocyte colonies from both r- and h-hep-mice, particularly in the former, at 3 and 11 weeks (termination phase), respectively (Figure 7, J and P). During the termination phase, m-HSCs in r-hepatocyte colonies from r-hep-mice were $TGF\text{-}\beta^+$ (Figure 7, J–L). However, importantly, m-HSCs in h-hepatocyte colonies of h-hep-mice were $TGF\text{-}\beta^-$ (Figure 7, P–R). HSCs that express TGF-β should be all m-HSCs in the chimeric mice, because the purity of the transplanted r- or h-hepatocytes was >99%. In r- and h-normal livers, $TGF\text{-}\beta^+$-HSCs were rarely observed (data not shown).

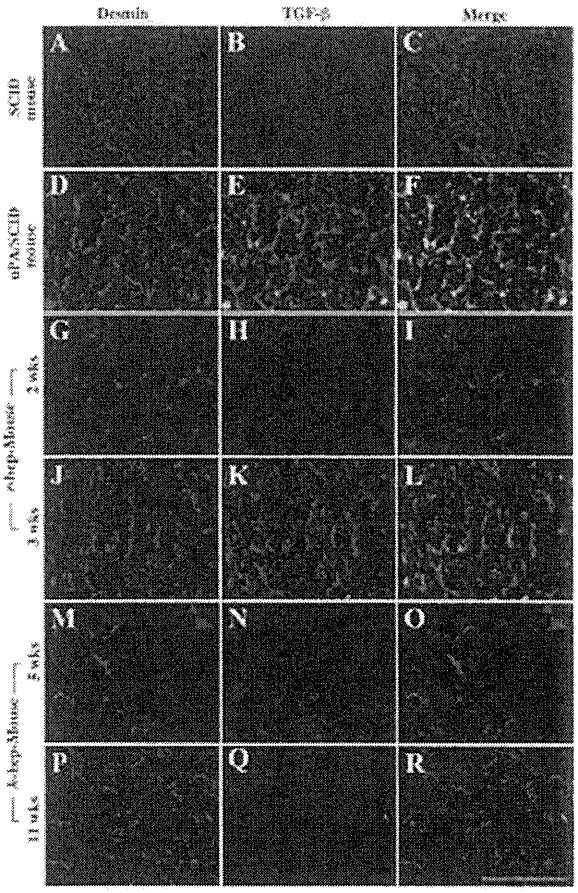

Figure 7. Expression and distribution of TGF-β in normal and chimeric mouse livers. Livers were removed, respectively, from 3-month-old wild-type SCID mice (**A–C**), 1-month-old uPA/SCID mice (**D–F**, injured region), r-hep-mice at 2 (**G–I**) and three (**J–L**) weeks after transplantation, and h-hep-mice at 5 (**M–O**) and 11 weeks (**P–R**). These livers were cryosectioned and double-immunostained for desmin (**A**, **D**, **G**, **J**, **M**, and **P**, red) and TGF-β (**B**, **E**, **H**, **K**, **N**, and **Q**, green). The two sets of photographs are merged and shown in the corresponding panels (**C**, **F**, **I**, **L**, **O**, and **R**) in the **right column**. Serial sections from r- and h-hep-mouse livers were immunostained for rRT1A and hCK8/18 to identify r- and h-hepatocytes, respectively (data not shown). Similar results were obtained from three different mice. Scale bar = 100 μm.

Smad proteins are major intracellular effectors in both TGFBR and ACVR signaling. The distributions of Smad2/3 were examined on liver sections prepared from r- and h-hep-mice at 3 and at 11 weeks (termination phase of r- and h-hep-mice, respectively), respectively, together with liver tissues from Fischer 344 rats and the 49YM donor as normal controls (Figure 8). The nuclei of normal r-livers (Figure 8, A and B) and h-livers (Figure 8, G and H) were both $Smad2^-/3^-$. In contrast, the nuclei of r-hepatocytes in r-hep-mouse were strongly $Smad2^+/3^+$ (Figure 8, D and E), supporting the evidence that r-hepatocytes are activated by TGF-β from m-HSCs. However, as expected, h-hepatocytes showed little or no Smad2/3 immunoreactivity (Figure 8, J and K), suggesting that